JOURNAL OF PETROLOGY

Journal of Petrology, 2020, Vol. 61, No. 6: egaa060
doi: 10.1093/petrology/egaa060
Advance Access Publication Date: 5 June 2020
Original Article

OXFORD

Various Ages of Recycled Material in the Source of Cenozoic Basalts in SE China: Implications for the Role of the Hainan Plume

Yan-Qing Li[1,2]*, Hiroshi Kitagawa [1], Eizo Nakamura[1], Changqian Ma[3], Xiangyun Hu[2], Katsura Kobayashi[1], and Chie Sakaguchi[1]

[1]Pheasant Memorial Laboratory, Institute for Planetary Materials, Okayama University at Misasa, 682-0193, Misasa, Tottori, Japan; [2]Institute of Geophysics & Geomatics, China University of Geosciences, Wuhan 430074, China; [3]State Key Laboratory of Geological Process and Mineral Resources, School of Earth Sciences, China University of Geosciences, Wuhan 430074, China

Corresponding author. E-mail: yanqingli@okayama-u.ac.jp

Received 23 November 2019; Accepted 31 May 2020

ABSTRACT

Subduction processes introduce crustal materials into the mantle, and mantle plumes return them to the surface. However, when and how the subducted materials were recorded in the plume-related basalts remains unclear. Here we investigate geochronology, bulk-rock composition, and Sr–Nd–Pb isotopes of Cenozoic basalts from Southeast China, occurring near the west Pacific subduction zone and the seismically detected Hainan plume. Volcanism beginning in the late Oligocene in the continental margin of SE China consistently becomes younger landward. Together with a compilation of published results on the synchronous basalts from the South China Sea seamounts and the Indochina peninsula, the volcanoes close to the Pacific subduction zone exhibit more radiogenic Pb and Sr isotopes associated with less radiogenic Nd isotopes compared with those of the inland volcanoes. Such spatiotemporal variations in radiogenic isotopes imply oceanic crusts of different ages in the source, each corresponding to a different geographical volcanic belt. Major-element features such as low CaO, high TiO_2 and high Fe/Mn ratios imply that pyroxenite/eclogite could serve as a source lithology of the SE China basalts. Specific trace-element signatures reveal the important roles of recycled oceanic crust along with surface sediment, which was inconsistently dehydrated during subduction. A geologically, geochemically, and geophysically plausible scenario is proposed to illustrate the time–space–source correlation of the late Cenozoic basaltic lavas in SE Asia. The Hainan plume delivered the ancient subducted crust (1·5 Ga) from the core–mantle boundary and, subsequently, the subducted Pacific plate crustal materials from the mantle transition zone to the shallow mantle as a result of mantle convection induced by continuous subduction of the Pacific plate. Such recycled materials of different ages contributed to the geographical compositional heterogeneities of the late Cenozoic basaltic lavas in SE Asia.

Key words: SE China; Cenozoic basalts; Hainan plume; recycled oceanic crust; petrogenesis

INTRODUCTION

Intra-plate basaltic volcanism, occurring in both oceanic and continental settings and including large-scale flood basalt eruption and small-volume monogenetic volcanism, is a widespread phenomenon on Earth (White, 2010; Smith & Németh, 2017). Such intra-plate volcanism typically occurs in settings located far from subduction zones, yet chemical and isotopic compositions of erupted products suggest involvement of subducted crustal materials in the mantle source (e.g. Chauvel & Hémond, 2000; Sobolev *et al.*, 2007; Heinonen *et al.*, 2014). Thus, the petrological and

geochemical signatures of intra-plate basaltic magmas document important information of crust–mantle mass exchange through the subduction system and mantle plumes (Hofmann & White, 1982; Wang *et al.*, 2013). However, the exact composition and nature of the subducted crustal materials in intra-plate lavas are still unclear (Stracke, 2012). Likewise, the geodynamic mechanism by which mantle upwellings or plumes originate remains elusive (Jackson *et al.*, 2017).

The geochemical similarities between some deep mantle-derived oceanic island basalts (OIB) and continental crust, oceanic crust and sedimentary material provide essential evidence that crustal materials transfer into the deep mantle via subduction and participate in the genesis of intra-plate basaltic magmas (Stracke *et al.*, 2003; Willbold & Stracke, 2006). OIB-like lavas show wide variations in isotope composition, and many of the variations are thought to reflect contributions from mantle reservoirs composed of distinct crustal components that have undergone time-integrated evolution over millions to billions of years (Tackley, 2011; Weis *et al.*, 2011; Hanyu *et al.*, 2014). Incorporation of crustal materials into magma source regions may occur in several ways. For instance, an ancient dehydrated oceanic crust has been widely invoked to explain the extremely radiogenic Pb isotope signatures of HIMU lavas [high-μ; $\mu = {}^{238}U/{}^{204}Pb$; characterized by radiogenic $^{206}Pb/^{204}Pb$ ($>20{\cdot}5$) and $^{207}Pb/^{204}Pb$ ($>15{\cdot}7$)] (e.g. Stracke *et al.*, 2003, 2005; Nebel *et al.*, 2013; Hanyu *et al.*, 2014; Castillo, 2015). Melting of metasomatized lithosphere, delaminated from the base of continental crust, has also been considered to produce the source of HIMU magmas (e.g. Scott *et al.*, 2016; Homrighausen *et al.*, 2018). Recycling ages of the crustal materials are also considered to be variable. For example, the HIMU signature is created by long-term (1–2 Ga) storage within the mantle, whereas a relatively young age ($<0{\cdot}5$–1 Ga) is considered to explain the isotopic signature in some hotspot magmas (e.g. 200 – 650 Ma for Hawaiian lavas; Sobolev *et al.*, 2011). These findings suggest that subducted oceanic crusts of various ages are ubiquitous in the mantle. In addition to considering the recycling ages, numerous crustal components with variable parent–daughter ratios have been invoked to explain the various isotopic features of intra-plate basaltic magmas. These include mid-ocean ridge basalt (MORB) (e.g. Sobolev *et al.*, 2011), lower oceanic crust (gabbro) (e.g. Gasperini *et al.*, 2000), marine sediments (Huang & Frey, 2005), continental crust (e.g. Gao *et al.*, 2004; Willbold & Stracke, 2006, 2010), and the delaminated sub-continental lithospheric mantle (SCLM) which has been broadly metasomatized by carbonatitic and/or silicate melts derived from subducted oceanic materials (Scott *et al.*, 2016; Weiss *et al.*, 2016; Homrighausen *et al.*, 2018). Chemical modification of subducted oceanic slab material, such as hydrothermal alteration and subsequent dehydration during subduction, which would considerably modify the initial parent–daughter ratios, has also been discussed (Pietruszka *et al.*, 2013; Hanyu *et al.*, 2014). Thus, a comprehensive evaluation of the geochemical characteristics of intra-plate basalts is essential to better understand the fate of subducted slabs in the mantle and the implications of crustal recycling for mantle heterogeneity (Eisele *et al.*, 2002; Nebel *et al.*, 2013).

Late Cenozoic intra-plate volcanism is widely distributed in East Asia, a part of the currently active, circum-Pacific volcanic belt (Fig. 1a.and b). These lavas generally have OIB-like trace element features (e.g. Ho *et al.*, 2003; Kuritani *et al.*, 2011; Li *et al.*, 2017*b*), and their isotopic compositions reveal prominent regional-scale variations in the source region. The basalts from North and NE China show isotopic affinities with EM1-type OIB (enriched mantle 1; intermediate $^{87}Sr/^{86}Sr$ and low $^{143}Nd/^{144}Nd$ and $^{206}Pb/^{204}Pb$), whereas those from SE China and Jeju island, an island located south of the Korean Peninsula, show EM2-type affinities (enriched mantle 2; high $^{87}Sr/^{86}Sr$ and intermediate $^{143}Nd/^{144}Nd$ and $^{206}Pb/^{204}Pb$) (Fig. 1a) (Zou *et al.*, 2000; Chen *et al.*, 2009; Brenna *et al.*, 2012*a*, 2012*b*). Basalts from the Korean Peninsula near the southern end of the Japan Sea show a transitional feature between EM1- and EM2-type OIB (Choi *et al.*, 2006). High-resolution seismic tomographic images for eastern China from 27°N to 41°N identified a high-velocity slab in the mantle transition zone (MTZ; depths of 410 – 660 km), which is thought to be a fragment of the subducted Pacific plate (Fig. 1c) (Huang & Zhao, 2006; Li & van der Hilst, 2010). Many studies have thus linked the origin of EM-like signatures of the Cenozoic basalts in East China to the stagnant Pacific slab in the deep mantle (e.g. Li *et al.*, 2015, 2016; Xu *et al.*, 2018).

However, the areas south of 27°N in East China do not show such a high-velocity anomalous belt in the MTZ (Fig. 1c). Instead, a continuous low-velocity column extending from the surface to 660 km depth beneath North Hainan Island and the Leizhou Peninsula (*c.* 20°N) is revealed by the surface-wave tomography (Lebedev & Nolet, 2003). More recently, regional travel-time tomography showed that the low-velocity anomalies were traceable from the surface to 1300 km depth beneath the Hainan region (Huang & Zhao, 2006), whereas the global tomographic models showed the low-velocity anomalies extending to about 1900 km depth or to the lowermost mantle (e.g. Montelli *et al.*, 2006). Meanwhile, basaltic lava flows are widely distributed and occupy an area of over 7000 km^2 in Hainan Island and the Leizhou Peninsula (Zou & Fan, 2010). These lavas have erupted since the late Oligocene (28 Ma; Sun, 1991) with magmatic pulses at 17–12 Ma (Zhu & Wang, 1989; Wang *et al.*, 2012), became widespread during the Pliocene (6–2 Ma), and reached a peak in the Pleistocene (<2 Ma; Zhou *et al.*, 1988; Ho *et al.*, 2000; Liu *et al.*, 2015). The extrusion rate during the Holocene is estimated to be 0·1–0·25 $km^3\,a^{-1}$ (Liu *et al.*, 2015), comparable with those of typical hotspots such as Hawaii (0·3–0·7 $km^3\,a^{-1}$; Vidal & Bonneville, 2004) and Iceland (0·1 $km^3\,a^{-1}$; Slater *et al.*, 1998). With

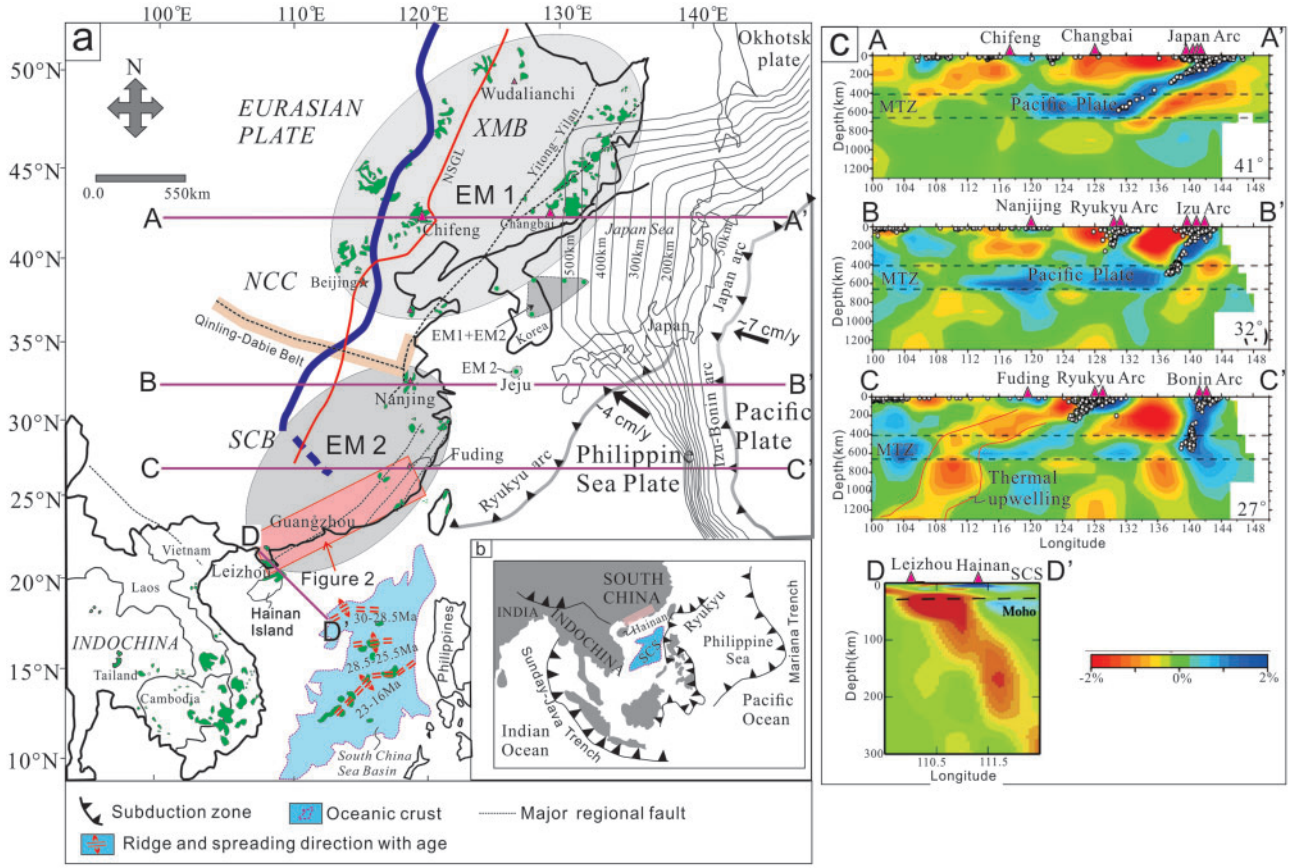

Fig. 1. (a) Simplified geological map of eastern Asia with distributions of Cenozoic basalts and the major regional faults (modified after Ho *et al.*, 2003; Choi *et al.*, 2006; Huang *et al.*, 2013; Li *et al.*, 2017*a*; Hoang *et al.*, 2018). The thin light gray lines with numbers denote the depth contours of the present upper boundary of the subducting Pacific slab estimated from seismicity (Liu *et al.*, 2017). The thick red line shows the boundary of the gravity anomaly in East China. The thick blue line represents the western edge of the flat slab in the mantle transition zone (MTZ) beneath East Asia, which was estimated from a tomographic model (Liu *et al.*, 2017). The continuous sawtooth lines denote the westward subduction zones of the Philippine Sea plate and the Pacific plate. The four purple lines with capitals at the beginning and the end denote locations of the vertical cross-sections shown in (c). The shaded areas represent the Cenozoic basalts in East China with EM1-type and EM2-type isotopic affinities (Zou *et al.*, 2000); the latter are also representative of the basalts from the Korean Peninsula (Choi *et al.*, 2006). The red rectangle shown enlarged in Fig. 2 indicates where the samples used in this study were taken from. XMB, Xing–Meng Block; NCC, North China Craton; SCB, South China Block; NSGL, North–South Gravity Linement. (b) The major subduction zones surrounding the margin of South China and the Indochina Peninsula (modified after Wang *et al.*, 2013; Zhang *et al.*, 2018). SCS, South China Sea. (c) Vertical cross-sections of P-wave tomography along the profiles in (a) (after Huang & Zhao, 2006; Lei *et al.*, 2009). The red and blue colors denote low and high velocity perturbations, respectively, as shown by the color bar with numbers below. The red triangles atop each cross-section denote the locations of Cenozoic volcanoes. The background seismicity of each profile is shown by white circles. The two dashed black lines denote the 410 and 660 km discontinuities of the MTZ. The flat high-velocity anomaly in the MTZ was interpreted as representing the stagnant Pacific plate beneath East Asia (e.g. Huang & Zhao, 2006), and the subvertical low-velocity anomaly crossing the MTZ into the upper mantle was interpreted as the thermal upwelling beneath the Hainan Island (e.g. Lei *et al.*, 2009).

excess mantle temperature of 140–200 °C (Wei & Chen, 2016), the lower-mantle-rooted, low-velocity seismic structure called the 'Hainan plume' is considered to have played a crucial role in the formation of the large-scale, contemporaneous basalts in SE Asia, including SE China, the Indochina peninsula and the South China Sea (Yan *et al.*, 2018; Yu *et al.*, 2018; Zhang *et al.*, 2018).

In addition, volcanism in SE Asia occurred at the margin of the subduction zones of the Pacific and Philippine Sea to the east and the Indo-Australian slab to the south and west (Fig. 1a and b). This complex and unique tectonic setting makes the SE Asia igneous province a model from which the potential association between mantle plumes, subducted oceanic materials, and mantle heterogeneity can be deduced. Elucidating such relationships should reveal the key processes that resulted in the Cenozoic tectono-magmatic regime in SE Asia and should have significant implications for understanding the dynamics of mantle geochemical cycling. Abundant geochemical data are available for the basalts associated with individual volcanoes in the regions (e.g. Zou *et al.*, 2000; Wang *et al.*, 2012, 2013; Huang *et al.*, 2013; Zeng *et al.*, 2017). Now a comprehensive study is required that combines the geochemical diversity with the temporal–spatial distribution of these Cenozoic basalts to elucidate the evolution of the source magma compositions and the tectonic evolution of the continental lithosphere beneath SE China.

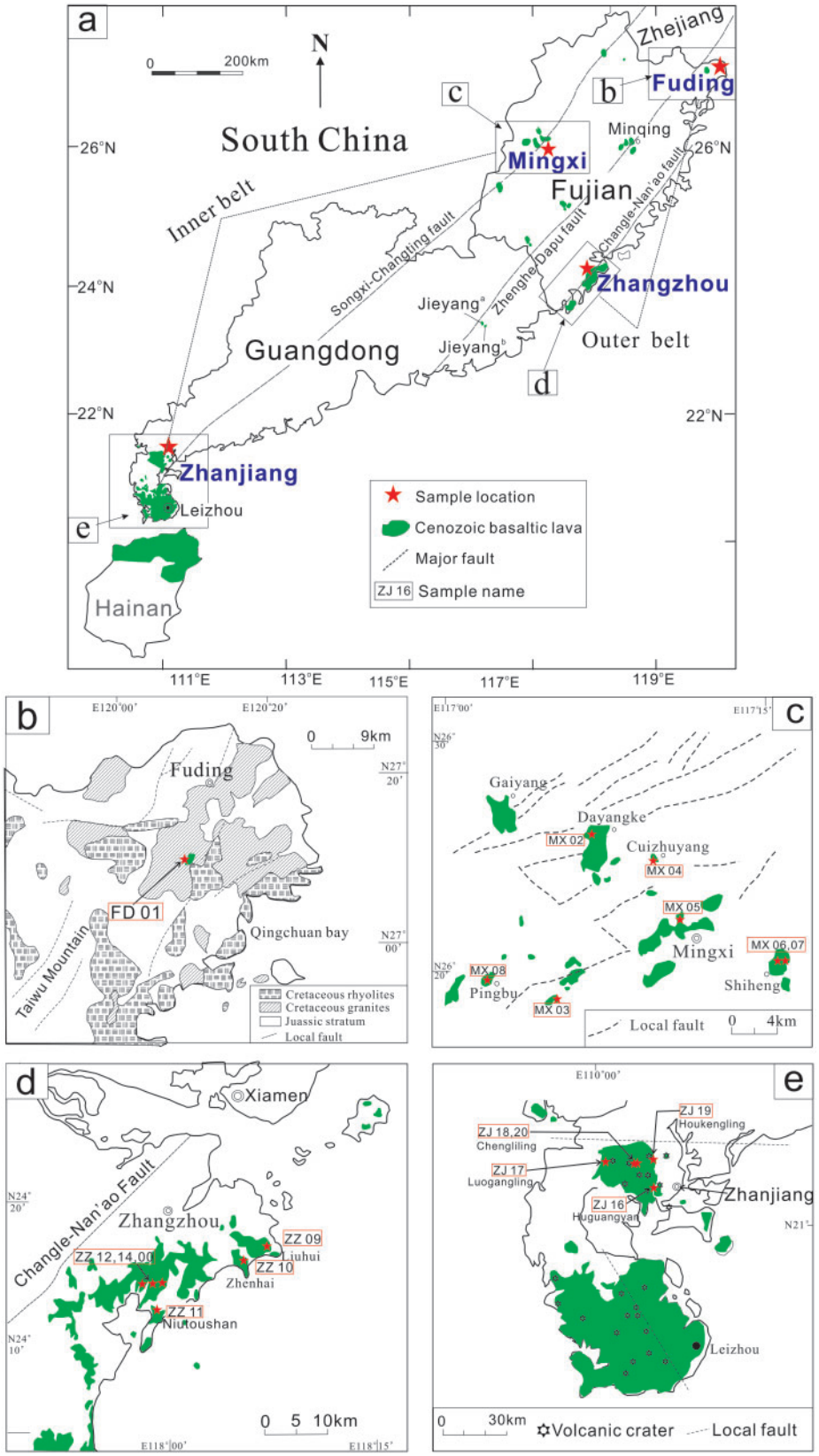

Fig. 2. (a) Sketch map of the distribution of Cenozoic basaltic lavas in Fujian and Guangdong Provinces (after Ho *et al.*, 2003). Several small-scale basaltic pipes were reported in Jieyang (Huang *et al.*, 2013). Here, we use superscript lowercase letters (i.e. Jieyang[a] and Jieyang[b]) to represent pipes with different eruption ages. Their eruption ages are shown in Fig. 3. (b–e) Enlarged maps of the areas where the samples were collected (modified after Chen & Zhang, 1992; Ho *et al.*, 2000; Zeng *et al.*, 2017). The red stars denote sample locations, and the sample names used in this study are shown in red rectangles. The detailed longitude and latitude values of sampling locations can be found in Supplementary Data Table S2.

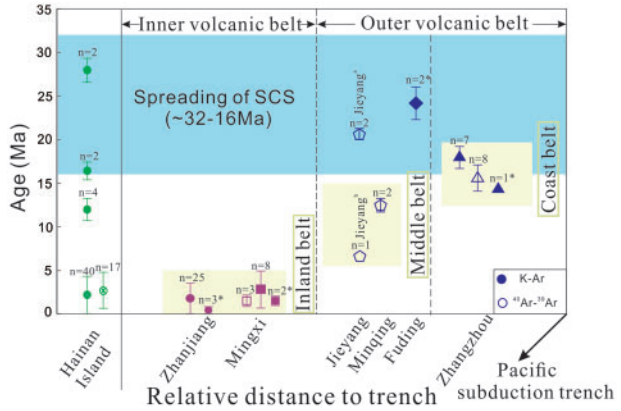

Fig. 3. Summary of the temporal and spatial variations of the late Cenozoic basalts in the Fujian–Guangdong areas. All the volcanoes are divided into three belts called the coast belt, the middle belt and the inland belt, according to the three subparallel major regional faults shown in Fig. 2a. Color codes: pink, lavas from the inner volcanic belt; blue, lavas from the outer volcanic belt; green, Hainan Island basalts. The filled and open symbols denote ages measured by the K–Ar and ^{40}Ar–^{39}Ar method, respectively. Numbers marked with an asterisk are the samples measured by this study. Error bars correspond to 2σ. The volcanic localities can be found in Fig. 2a. Radiometric age data are compiled from Ge *et al.* (1989), Zhu & Wang (1989), Sun (1991), Chen & Zhang (1992), Juang & Ho (1996), Ho *et al.* (2000, 2003) and Huang *et al.* (2013). Ages of the basalts from Hainan Island are also shown for comparison, and are from Ho *et al.* (2000) and Wang *et al.* (2012). SCS, South China Sea.

In this study, we present a comprehensive set of whole-rock geochemical, Sr–Nd–Pb isotope and K–Ar geochronological data for SE China basalts, and use these data to investigate the relative contributions of subducted material to the potential geochemical reservoirs in the mantle source region. Combined with a compilation of published data from Hainan Island, the Indochina peninsula and the South China Sea seamount basalts, we elucidate the geodynamic processes that gave rise to the spatial geochemical distributions in these lavas, and provide the geochemical evidence for the geophysical anomalies beneath this region. On the basis of our results, we present a geologically, geochemically, and geophysically plausible scenario to illustrate the time–space–source correlation of the late Cenozoic basaltic lavas.

GEOLOGICAL BACKGROUND AND SAMPLING

Cenozoic intra-plate basaltic volcanoes in SE China are widely distributed in Fujian, Guangdong and Hainan Provinces (Fig. 2) (Ho *et al.*, 2003). However, these continental margin volcanoes are thousands of kilometers from the modern trenches of the Pacific subduction zone (e.g. Mariana trench) (Liu *et al.*, 2017). Moreover, global seismic tomography does not detect a downgoing slab beneath East China; instead, the subducted Pacific slab is flat-lying in the MTZ (Fig. 1c) (Huang & Zhao, 2006). Therefore, the Cenozoic volcanoes in SE China are generally defined as intra-plate volcanism (Xu *et al.*, 2018). The volcanism occurred in three NE-trending belts from the coastal to the inland areas, which are associated with three major regional faults (Zou *et al.*, 2000). Samples used in this study have covered these three volcanic belts. The Zhangzhou basalts erupted along the coast belt, Fuding basalts occurred along the middle belt, and Mingxi and Zhanjiang lavas appeared along the inland belt (Fig. 2).

About 20 years ago a plume was proposed beneath the Leizhou Peninsula and northern Hainan Island on the basis of global seismic tomographic studies, one of the few postulated to rise from the lower mantle (Zhao, 2007). Additionally, a thinner-than-normal MTZ and thickened crust beneath this region detected by recent seismic studies strongly supports the presence of the Hainan plume by suggesting that hot materials from the lower mantle penetrate through the MTZ, causing the 410 km discontinuity to be deeper and the 660 km discontinuity shallower. Thus, it is thought that the plume brings mantle materials to shallow depths causing further thickening of the crust (Wei & Chen, 2016). Thermal variations in the Hainan plume estimated from the tomography show that the temperature of the MTZ beneath the region is about 170–200 °C hotter than the surrounding mantle. This finding agrees well with the high mantle potential temperature of 1440–1550 °C calculated by the Hainan basalts (Wang *et al.*, 2012). Furthermore, the Hainan plume model is consistent with large-scale surface uplift since the late Neogene in the Indochina peninsula and from the Oligocene to *c.* 5 Ma in southern Hainan Island (Wang *et al.*, 2013).

In relation to the age of spreading in the South China Sea (SCS) (*c.* 32–16 Ma; Briais *et al.*, 1993; Li *et al.*, 2014*a*), the Cenozoic volcanic activity in SE China can be divided into three episodes (Xu *et al.*, 2012): (1) pre-spreading volcanism that produced voluminous OIB-type and island arc basalt (IAB)-type lavas; (2) syn-spreading volcanism, which ceased during the Oligocene to Early Miocene, that produced rare, isolated basaltic volcanoes in Guangdong (Jieyang; Huang *et al.*, 2013), Fujian (Fuding; present study), and the North Hainan Provinces at 32–22 Ma (Sun, 1991); (3) post-spreading volcanism, which began at *c.* 17 Ma in Zhangzhou and continued to 0·1 Ma in Zhanjiang (Ho *et al.*, 2003; present study). The major eruption period in Hainan Island is younger than 5 Ma (Zou & Fan, 2010), and the widespread volcanic activity in the Indochina peninsula is younger than 16 Ma (Hoang *et al.*, 2018). Volcanic seamounts in the SCS erupted after spreading of the SCS seafloor ceased, showing hotspot activities that may have been associated with the Hainan plume (Yan *et al.*, 2008; Zhang *et al.*, 2018).

The 40 basalt samples used in this study were collected from Fuding, Zhangzhou, Mingxi, and Zhanjiang in SE China (Fig. 2). All samples are porphyritic with phenocrysts of olivine (5–8 vol%) and clinopyroxene (1–4 vol%). Some of the Fuding basalts also contain phenocrysts of plagioclase (~2 vol%). The samples have intersertal to intergranular groundmasses consisting of

acicular plagioclase, microlitic clinopyroxene, minor olivine, Fe–Ti oxide, and interstitial glass. Detailed petrographic descriptions are given in the Supplementary Data (supplementary data are available for downloading at http://www.petrology.oxfordjournals.org).

WHOLE-ROCK GEOCHRONOLOGY AND GEOCHEMISTRY

All analyses were performed at the Pheasant Memorial Laboratory, Institute for Planetary Materials, Okayama University at Misasa, Japan, following the procedures of Nakamura *et al.* (2003). Details of analytical procedures for K–Ar dating and measurements of major oxides, trace elements and Sr–Nd–Pb isotopes are presented in the Supplementary Data.

K–Ar ages

The K–Ar ages of the fresh samples are given in Supplementary Data Table S1 and plotted with previously published data in Fig. 3. Our dating results are consistent with the previously published data for samples from the same locality (Ge *et al.*, 1989; Sun, 1991; Chen & Zhang, 1992; Juang & Ho, 1996; Ho *et al.*, 2000, 2003; Huang *et al.*, 2013). Most of the basaltic lavas reported here were erupted after spreading of the SCS seafloor ceased; only those from Fuding (22·3 and 26·0 Ma) are syn-spreading lavas.

The post-spreading (<16 Ma) basaltic lavas occurring along two regional faults become progressively younger from coastal to inland fault (Fig. 3). The coastline of SE China is sub-parallel to the Pacific subduction trench (Fig. 1b), so the distance from the volcanoes to the coastline is proportional to the relative distance to the Pacific subduction zone. The ages range from 15 Ma for a sample from Zhangzhou to 2·1–1·3 Ma for samples from Mingxi, a distance of ~270 km when measured perpendicular to the coast. The youngest lavas (*c.* 0·1 Ma), which erupted along the southwestern extension of the inland rift, are from Zhanjiang (Fig. 2a). Based on the relative distance to the Pacific subduction zone, we divided the studied samples into an outer volcanic belt (Fuding and Zhangzhou) and an inner volcanic belt (Mingxi and Zhanjiang) (Fig. 3).

Major oxides and trace elements

New major oxide and trace element data for the samples in SE China are given in Supplementary Data Table S2. The bulk-rock chemical compositions of samples in this study were plotted with those from nearby areas in SE Asia, such as Jieyang, Hainan Island and the Indochina peninsula (Figs 4 and 5) (Wang *et al.*, 2012; Huang *et al.*, 2013; An *et al.*, 2017; Hoang *et al.*, 2018).

The samples show a considerable range in composition (SiO_2 = 40·4–53·0 wt% and $Na_2O + K_2O$ = 2·8–6·7 wt%) and were classified as foidite, basanite, trachybasalt, basaltic trachyandesite, basalt, and basaltic andesite (Fig. 4). The term 'basalt' is employed in a general sense in this study to encompass the above rock types. From the total alkalis–silica (TAS) diagram, the syn-spreading lavas (Fuding and Jieyang) are alkali basalts, and the post-spreading lavas vary from basanites to alkali and sub-alkali basalts. Hainan lavas are dominated by tholeiites with subordinate alkali basalts. Both MgO and FeO^T have relatively high, but variable values (8·1–13·4 wt% and 5·9–11·8 wt%, respectively), yielding Mg-numbers [100Mg/(Mg + Fe^{2+}), assuming $Fe^{2+} = 0{\cdot}85Fe_{tot}$] ranging from 55 to 68. The major oxide compositions of these samples overlap with those of Cenozoic basalts from other localities in SE Asia. The basanites from Mingxi, Fuding and Jieyang have higher MgO and CaO/Al_2O_3 ratios and lower SiO_2 and Al_2O_3 contents than those from Zhanjiang and Zhangzhou (Fig. 5a, b and g). The Zhanjiang and Hainan lavas become compositionally closer as the distance between them decreases. The Fuding and Jieyang lavas, which erupted along the same fault, at a similar distance from the western Pacific subduction zone, plot close together in the Harker diagrams (Fig. 5), reflecting that the major oxide compositions in the lavas of the two localities are almost indistinguishable.

Trace element concentrations in the lavas vary with rock type, being higher in the basanites than in the mildly alkaline basalts and tholeiites. In a primitive mantle-normalized, multi-element plot, the lavas show OIB-like features such as enrichment of most of the incompatible elements including large ion lithophile elements (LILE) (e.g. Rb, Ba, Th, U) and light rare earth elements (LREE) (Fig. 6a–d). In chondrite-normalized REE patterns, the lavas exhibit enriched LREE relative to heavy rare earth elements (HREE), and do not display negative Eu anomalies (Fig. 6e–h). All of the lavas are also

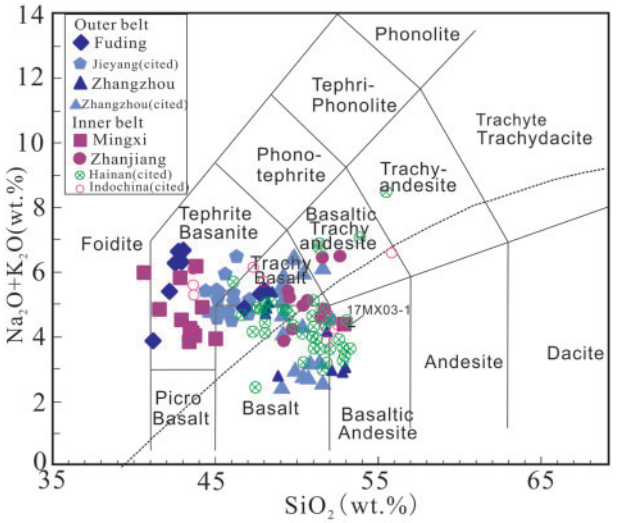

Fig. 4. Rock classification diagram of the basaltic rocks from this study, according to their $Na_2O + K_2O$ and SiO_2 contents, after Le Maitre *et al.* (2005). The dashed line separating alkaline and sub-alkaline basalts is from McDonald & Katsura (1964). The compiled data for the SE Asian basalts in previous studies are shown in Supplementary Data Table S8.

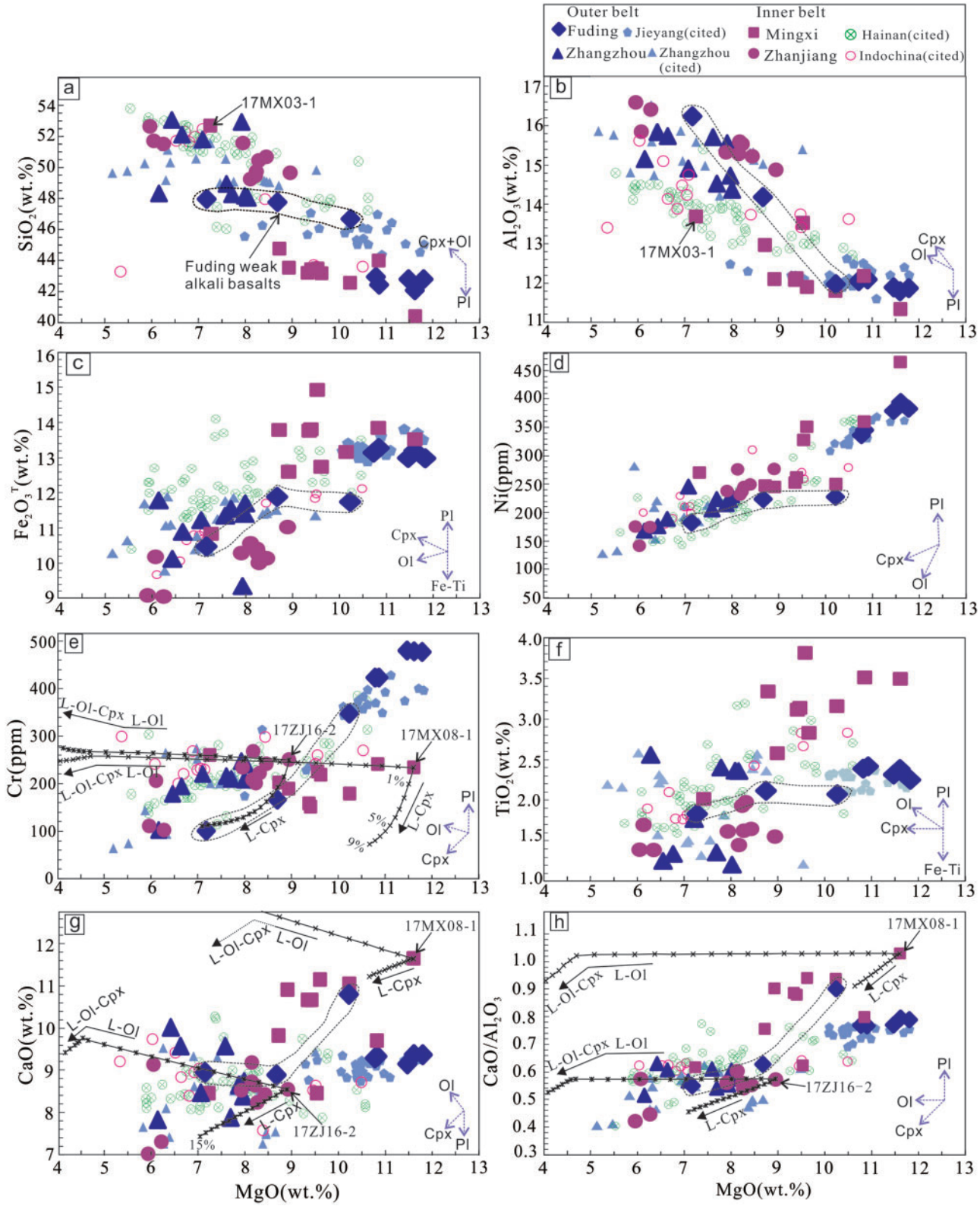

Fig. 5. Variations in (a) SiO_2, (b) Al_2O_3, (c) $Fe_2O_3^T$, (d) Ni, (e) Cr, (f) TiO_2, (g) CaO, and (h) CaO/Al_2O_3 vs MgO content for the basaltic rocks in SE China. Three analyzed samples (17FD01-8, 17MX07-1, 17MX07-3) with high LOI values >3 wt% were not included in this figure. The data for basalts from SE Asia compiled from previous studies are shown for comparison. The data sources are available in Supplementary Data Table S8. Fractionation vectors for olivine (Ol), clinopyroxene (Cpx), plagioclase (Pl) and Fe–Ti oxides are indicated. Fractional crystallization paths shown in (e), (g) and (h) are modelled by the Petrolog 3 program (Danyushevsky & Plechov, 2011), and represent the liquid (L) lines of descent for the starting materials (17MX08-1 and 17ZJ16-2) that crystallize Cpx (L-Cpx) or a crystal assemblage of Ol and Cpx (L-Ol-Cpx). Crosses or asterisks on the modeled paths correspond to 1 wt% fractionation intervals. Olivine–melt and clinopyroxene–melt equilibrium models are from Herzberg & O'Hara (2002) and Danyushevsky (2001), respectively. The default value 100 % is assigned to the extent of fractionation for each mineral, corresponding to the case of pure fractional crystallization. We modeled the crystal fractionation at 5 kbar and 3 kbar initial pressure for the Mingxi basanite (17MX08-1) and Zhanjiang basalt (17ZJ16-2), respectively. Water content was set as 0 wt% in the starting compositions.

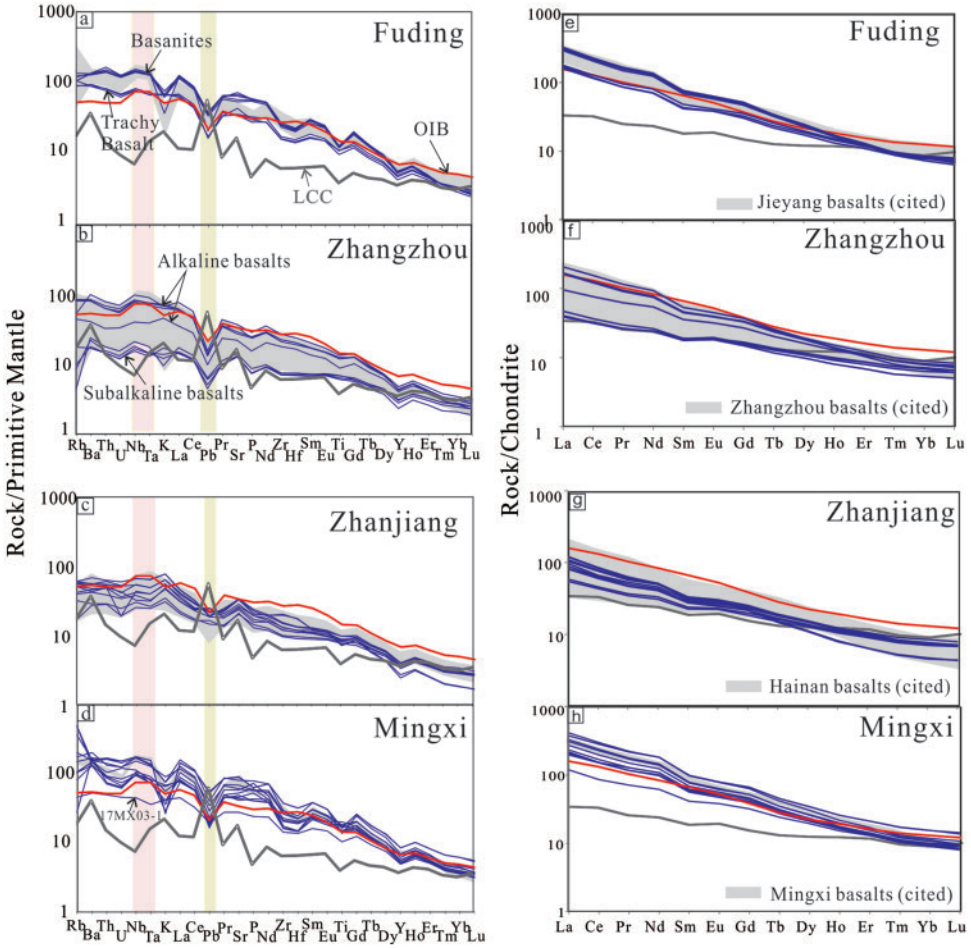

Fig. 6. (a–d) Primitive mantle-normalized (McDonough & Sun, 1995) multi-element plots; (e–h) chondrite-normalized (Sun & McDonough, 1989) rare earth element patterns of the basaltic rocks in SE China. The reference values of oceanic island basalts (OIB, red line) and lower continental crust (LCC, gray line) are from Sun & McDonough (1989) and Rudnick & Gao (2003), respectively. The gray shaded areas represent the trace-element abundances of the basalts from nearby areas, and the data sources are shown in Supplementary Data Table S8.

characterized by slightly enriched Nb and Ta relative to the neighboring elements, and negative Pb anomalies in the primitive mantle-normalized trace-element patterns (Fig. 6a–d). From the multi-element plots, it is also evident that lavas from each locality exhibit different K anomalies. The basanites from Mingxi and Fuding show distinctly negative K anomalies, lavas from Zhanjiang have slightly positive K anomalies, and the rest of the lavas display slightly negative K anomalies. In addition, the lavas studied here are rich in Sr, as manifested by slightly to distinctly positive Sr anomalies in the trace-element patterns. As with the major oxides, the trace elements in the Zhanjiang samples resemble those in Hainan Island lavas, displaying weakly negative Pb anomalies and distinctly positive Sr anomalies relative to the basaltic lavas from the other localities. Similarly, the Fuding lavas basically overlap the Jieyang lavas, and the trace elements of Zhangzhou lavas show many similarities to previously published data. Notably, rocks from Zhanjiang do not exhibit obvious negative Pb anomalies, and thus have lower Ce/Pb ratios (10·4–18·9) than the other analyzed samples (18·8–44·9).

Sr–Nd–Pb isotopes

The Sr–Nd–Pb isotope compositions analyzed in this study along with previously published data for basalts in SE Asia are illustrated in Fig. 7 and presented in Supplementary Data Tables S3 and S8. Hereafter, the $^{87}Sr/^{86}Sr$, $^{143}Nd/^{144}Nd$, $^{206}Pb/^{204}Pb$, $^{207}Pb/^{204}Pb$, and $^{208}Pb/^{204}Pb$ values of the basalts in this study refer to the initial ratios calculated on the basis of their eruption age and ratios of parent- and daughter-element abundances.

The isotopic data obtained in this study are consistent with the published data for the basaltic lavas from the same areas (Zou *et al.*, 2000; Han *et al.*, 2009; Sun *et al.*, 2017; Zeng *et al.*, 2017). Although the range of Sr–Nd isotope compositions may overlap, most samples from different localities have distinct isotope features. The rocks from the outer belt have lower $^{143}Nd/^{144}Nd$ [0·51279–0·51285, $\varepsilon_{Nd}(t) = 3{\cdot}3–4{\cdot}7$] than those from the inner belt [0·51284–0·51300, $\varepsilon_{Nd}(t) = 4{\cdot}0–7{\cdot}1$, except for

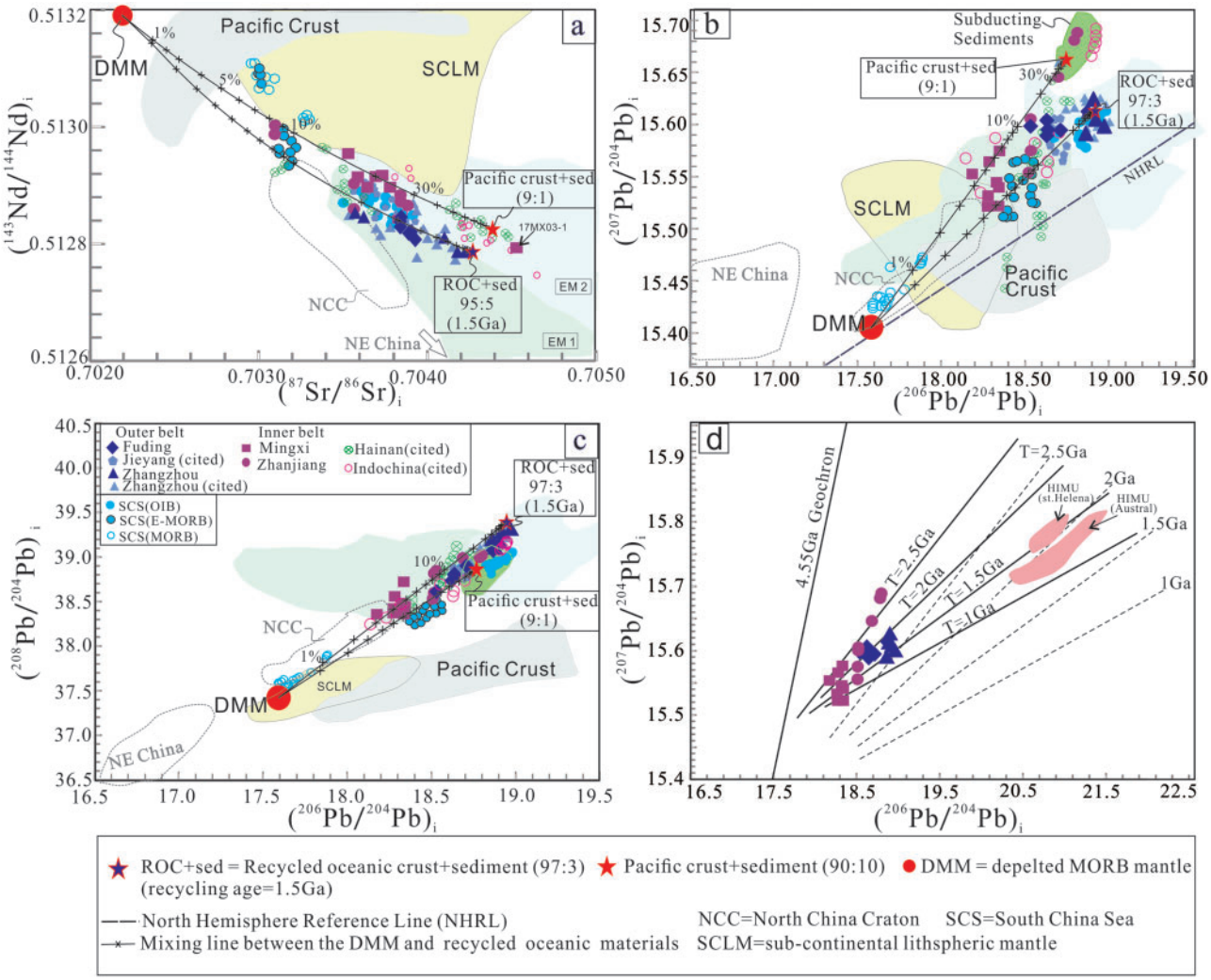

Fig. 7. Variations of (a) $(^{143}Nd/^{144}Nd)_i$ vs $(^{87}Sr/^{86}Sr)_i$, (b) $(^{207}Pb/^{204}Pb)_i$ vs $(^{206}Pb/^{204}Pb)_i$, and (c) $(^{208}Pb/^{204}Pb)_i$ vs $(^{206}Pb/^{204}Pb)_i$ for the basaltic lavas from SE China. The compiled data for the basaltic lavas from SE Asia shown for comparison are available in Supplementary Data Table S8. All the values used here are initial ratios calculated on the basis of their eruption age. Continuous lines denote the mixing lines between depleted MORB mantle (DMM) and recycled oceanic material. Recycled oceanic material results from the mixing of the recycled oceanic crust (ROC) and sediment components in various mixing proportions. Mixing lines are marked in 1 % increments from 1 to 10 %, and in 10 % increments from 10 to 100 %. Isotopic compositions of DMM are shown in Supplementary Data Table S5. The data source for the western Pacific crust values is shown in Supplementary Data Table S6, and subducting sediment values from the Mariana trench are shown in Supplementary Data Table S7. The parameters used to calculate the isotopic compositions of the 1·5 Ga recycled oceanic crust and sediments can be found in Supplementary Data Tables S4 and S5. The values for the subcontinental lithospheric mantle (SCLM) beneath SE China are from Tatsumoto *et al.* (1992) and Qi *et al.* (1995). The plotted regions for EM1- and EM2-type OIB are from Stracke *et al.* (2003), and for the North and NE China basalts are from Kuritani *et al.* (2011), Zeng *et al.* (2011) and the references therein. (d) The calculated present-day $^{206}Pb/^{204}Pb$ and $^{207}Pb/^{204}Pb$ ratios of ROC as functions of μ_{ROC} ($^{238}U/^{204}Pb$) and T_{ROC} (recycling age of ROC). Continuous lines denote isopleths for fixed initial μ_i = 8·2, and T_{ROC} (= 1, 1·5, 2 and 2·5 Ga) with different μ_{ROC}; dashed lines are shown for comparison with initial μ_i = 8·0. Additional explanations for the calculation can be found in the main text. The plot regions of HIMU lavas from St Helena and Austral are from Hanyu *et al.* (2014).

sample 17MX03-1]. The Jieyang basalts show higher $^{143}Nd/^{144}Nd$ than the Fuding basalts, but have similar Pb isotopic ratios (Fig. 7a and b). Overall, $^{143}Nd/^{144}Nd$ correlates negatively with $^{87}Sr/^{86}Sr$ ratios, and isotopic compositions in each region are more homogeneous than the Hainan and Indochina basalts, regardless of their major oxide compositions. The basalts of the SCS show large variations in Sr–Nd–Pb isotope compositions. The enriched (E)-MORB-type basalts show similar Sr–Nd–Pb isotope compositions to the Hainan basalts, and the OIB-type basalts display more enriched Sr–Nd isotopic signatures and have distinctly higher Pb isotopic components than the MORB-type basalts (Fig. 7a–c).

The $^{206}Pb/^{204}Pb$ ratios of the outer belt rocks (18·53–18·97) are more radiogenic than those of the inner belt

(18·18–18·80). At a given $^{206}Pb/^{204}Pb$, the Zhanjiang basalts show significant variation in $^{207}Pb/^{204}Pb$ ratios (Fig. 6b and c), as previously reported for the Hainan Island and Indochina basalts (Wang *et al.*, 2013).

DISCUSSION

Evaluating differentiation processes

Before using the bulk-rock geochemical compositions of basaltic rocks to infer their parental magma compositions, other factors occurring during and after magma ascent, such as alteration, crustal contamination, and fractional crystallization must be evaluated.

Post-eruptive alteration

One of the most common alteration processes occurring after eruption is fluid–rock interaction, which results in the loss or gain of fluid-mobile elements (Moon & Jayawardane, 2004). Highly incompatible and fluid-mobile elements such as Th, La, U, K and Rb may be more susceptible to basalt weathering than less mobile elements such as Nb (Xu *et al.*, 2005). The good correlations in the abundance of Nb and La as well as U and Th in the samples suggest little or no modification of these elements by subaerial weathering (Fig. 8a–c). Most samples in this study show low loss on ignition (LOI) values (<3 wt%), except for three samples (17FD01-8, 17MX07-1, 17MX07-3) (Supplementary Data Table S2). To avoid the equivocal evaluation for the source magma, we will avoid using the major oxide contents of these three samples in the following discussion, as the major oxide contents are strongly affected by the LOI values. Trace element ratios sensitive to weathering, such as Cs/Rb, do not correlate with LOI values (Fig. 8d), implying that the ratios of fluid-mobile elements in the studied lavas have been little affected by chemical weathering. Therefore, we conclude that the compositions of most of the lavas included in this study have been minimally affected by post-eruptive alteration.

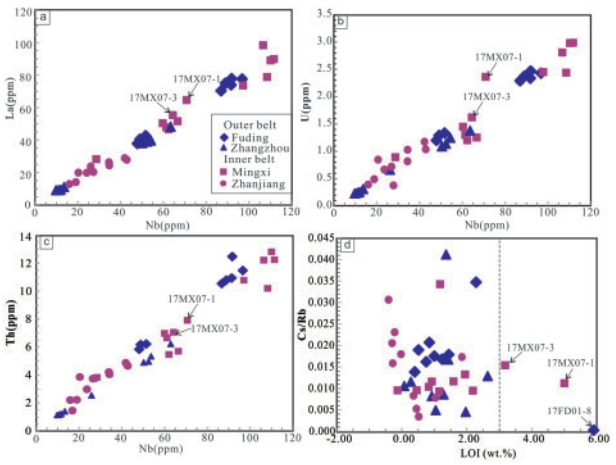

Fig. 8. Variations of (a) La, (b) U, and (c) Th vs Nb, and (d) Cs/Rb vs LOI values for the basaltic lavas in SE China.

Crustal contamination

Continental-crust contamination should result in higher SiO_2 and $^{87}Sr/^{86}Sr$ ratios, along with lower MgO and $^{143}Nd/^{144}Nd$ ratios in basaltic magmas. The lack of negative correlations between MgO and $^{87}Sr/^{86}Sr$ ratios and between SiO_2 and $^{143}Nd/^{144}Nd$ ratios in most of the samples (except for the Mingxi lavas) implies negligible upper continental crust (UCC) contamination (Fig. 9a and d). Meanwhile, the lavas from Zhangzhou and Zhanjiang generally show a negative correlation between SiO_2 content and $^{87}Sr/^{86}Sr$ ratio (Fig. 9c), which is different from what is expected for contamination from the UCC. The large variation of MgO contents in the lavas studied here does not correlate with $^{143}Nd/^{144}Nd$ ratios, implying an insignificant effect from crustal contamination, as the crustal contamination would cause an obviously positive correlation between these two values (Fig. 9b). Furthermore, the lower continental crust (LCC), composed of mafic rocks, has SiO_2 content and $^{87}Sr/^{86}Sr$ ratio comparable with basaltic lavas (Huang *et al.*, 2004; Ying *et al.*, 2010), which creates difficulties for evaluating LCC assimilation processes of mantle-derived magmas. The LCC beneath SE China, which is different from the UCC that has similar $^{206}Pb/^{204}Pb$ ratios to the lavas included in this study, is represented by granulite xenoliths in the basalts and shows distinctly lower $^{206}Pb/^{204}Pb$ ratios. The relatively narrow range of $^{206}Pb/^{204}Pb$ ratios in the lavas included in this study indicates a negligible role of the LCC in either the source region or during magma ascent (Fig. 9e). Similarly, the generally negative correlation between the $^{143}Nd/^{144}Nd$ and $^{206}Pb/^{204}Pb$ ratios further suggests a minimal effect of the LCC on magma generation.

The continental crust is also characterized by significant high field strength element (e.g. Nb, Ta, Zr and Hf) depletion and LILE enrichment. For example, average continental crust has La/Nb of ~2·5, normal (N)-MORB has La/Nb of ~1·0, and oceanic island basalts have La/Nb $\leq$ 1·2 (McDonough & Sun, 1995; Rudnick & Gao, 2003). The undepleted Nb and Ta abundances shown in the primitive mantle-normalized multi-element diagram (Fig. 6), indicated by low La/Nb ratios (0·66 – 0·98), and the lack of correlation between $^{87}Sr/^{86}Sr$ and La/Nb ratios, argue against contamination of a significant amount of continental crust (Gao *et al.*, 2017). In addition, the generally negative correlation between $^{143}Nd/^{144}Nd$ and Sm/Nd (Fig. 9f) contrasts with continental crust contamination, as addition of continental crustal components to a mantle-derived magma could decrease both Sm/Nd and $^{143}Nd/^{144}Nd$ ratios. However, it should be noted that one sample (17MX03-1) shows obviously higher SiO_2, Sm/Nd, La/Nb (1·0) and $^{87}Sr/^{86}Sr$ ratios, and more depleted Nb and Ta concentrations with a low $\varepsilon_{Nd}(t)$ value, compared with those of the other Mingxi lavas, and may thus have received some crustal input. The overall constant Nb/U ratios (average = 41) fall in the range defined by OIB and MORB (47 ± 10), further supporting insignificant crustal

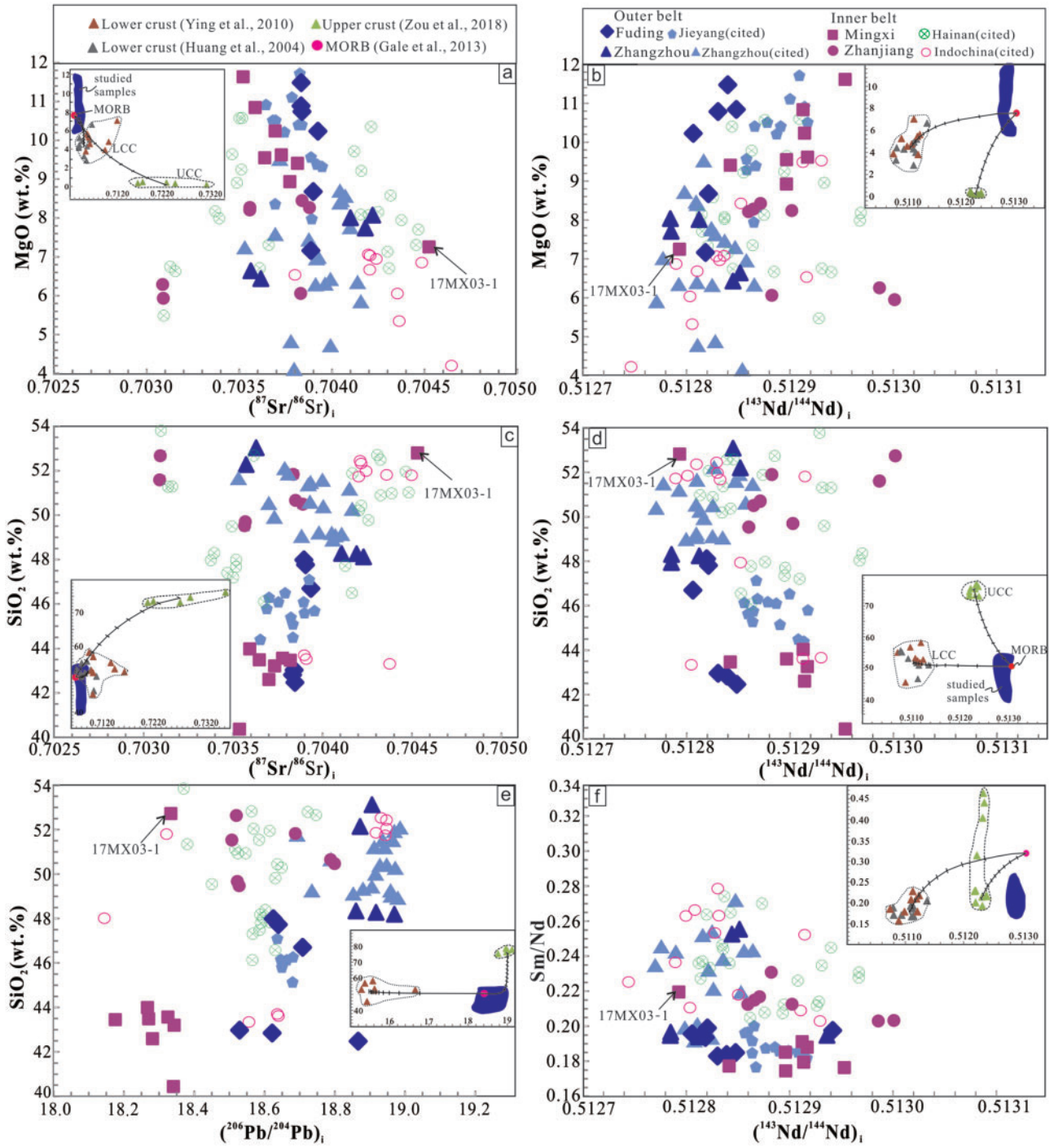

Fig. 9. Variations of (a) MgO vs $(^{87}Sr/^{86}Sr)_i$, (b) MgO vs $(^{143}Nd/^{144}Nd)_i$, (c) SiO_2 vs $(^{87}Sr/^{86}Sr)_i$, (d) SiO_2 vs $(^{143}Nd/^{144}Nd)_i$, (e) SiO_2 vs $(^{206}Pb/^{204}Pb)_i$, and (f) Sm/Nd vs $(^{143}Nd/^{144}Nd)_i$ for the basaltic lavas from SE China. Compiled data for the SE Asia basalts are shown in Supplementary Data Table S8. Insets schematically show the mixing trends between MORB and continental crustal components (LCC, lower continental crust; UCC, upper continental crust). Mixing lines are marked in 10 % increments. Data source for the granulite xenoliths hosted in Cenozoic basalts from East China, which represent the LCC component, are from Huang *et al.* (2004) and Ying *et al.* (2010). Mesozoic granites from SE China are used to represent the component of UCC, and the data for these are from Zhou *et al.* (2018). Compositions of MORB used for the mixing calculation are from Gale *et al.* (2013).

contamination. Furthermore, the common occurrence of peridotite xenoliths in the studied rocks indicates that the magmas ascended rapidly, allowing limited opportunity for contamination.

Fractional crystallization

The large variation of MgO contents in the SE China basaltic lavas studied here may record fractional crystallization processes after the magma formation. This is

consistent with the petrographic observation that olivine, clinopyroxene and to a lesser extent plagioclase are the common phenocrysts in the studied samples. The overall negative correlations of SiO_2 and Al_2O_3 (Fig. 5a and b) and positive correlations of $Fe_2O_3^T$ and Ni (Fig. 5c and d) with MgO suggest some fractional crystallization of olivine from the basaltic magmas. However, the relationships between MgO and Cr, CaO and TiO_2 contents and CaO/Al_2O_3 ratios in all the samples are significantly scattered and do not lie on the single liquid line of descent (Fig. 5e–h). The extents of variation in major-element abundances differ in volcanic fields. For instance, the Fuding lavas have a large variation in Cr abundance, which correlates positively with MgO, whereas lavas from the other localities show relatively constant Cr content (Fig. 5e). The CaO and TiO_2 abundances and CaO/Al_2O_3 ratios of the Mingxi lavas are obviously higher than those in the Fuding lavas at comparable MgO contents (Fig. 5f–h). In the low-Mg suites (Zhanjiang and Zhangzhou lavas), the variations of SiO_2, $Fe_2O_3^T$, TiO_2, CaO and CaO/Al_2O_3 show poor correlations with MgO (Fig. 5a, c and f–h). Such scattered trends in Harker diagrams imply that the SE China basalts were not derived from a single parental magma. In the following, we will discuss the effect of fractional crystallization on whole-rock major oxide variation within each volcanic field.

Among the lavas from Fuding, the basanites have high MgO (>10 wt%) and Ni (>280 ppm) abundances, which are close to those of the primitive magmas derived from the mantle (Brenna *et al.*, 2012*a*). From basanites toward weakly alkaline basalts, olivine is a dominant phase as suggested by an increase of CaO and decreases of $Fe_2O_3^T$ and Ni with decreasing MgO (Fig. 5a, d and g). Then, clinopyroxene participated in crystallization, resulting in increases of SiO_2 and Al_2O_3 (Fig. 5a and b) and decreases of CaO, CaO/Al_2O_3 and Cr with falling MgO among the weakly alkaline basalts (Fig. 5e, g and h). Inflection of Ni–MgO correlation at MgO 10–11 wt% is also consistent with cotectic relationship of these two phases.

Except for crustally assimilated 17MX03-1, the Mingxi lavas show slight increases in SiO_2 and Al_2O_3 and decreases in Ni, CaO and CaO/Al_2O_3 with falling MgO (Fig. 5 a, b, d, g and h). These features suggest some degree of clinopyroxene fractionation. However, the relatively constant Cr abundance with decreasing MgO is inconsistent with the scenario that clinopyroxene acts as the predominant fractional phase (Fig. 5e). To further constrain the fractional mineral assemblage and the relative proportion of mineral phases in the Mingxi lavas, we utilized the PETROLOG 3 algorithm (Danyushevsky & Plechov, 2011). The results are shown in Fig. 5e, g and h, and the detailed parameters set in the software can be found in the figure caption.

Sample 17MX08-1 with the highest MgO content (11·6 wt%) and Ni abundance (415 ppm) was chosen as the starting material. According to the model, 9 % fractional crystallization of clinopyroxene will exhaust the Cr of the primary magma (Fig. 5e), because Cr is highly compatible in clinopyroxene ($D_{Cr}^{Cpx/melt} > 7$; Skulski *et al.*, 1994). The correlation between Cr and MgO is apparently inconsistent with the modelled trend formed by clinopyroxene fractionation. On the other hand, if clinopyroxene fractionation occurs after the primary magma has evolved to a derivative lava by olivine fractionation (Herzberg *et al.*, 2007), the positive correlations of CaO and CaO/Al_2O_3 with MgO are inconsistent with the initial crystallization of olivine (Fig. 5g and h). Meanwhile, the weakly positive correlation between TiO_2 and MgO contents (Fig. 5f) may not result from Fe–Ti oxide crystallization, because removal of Fe–Ti oxides should cause a significant decrease of TiO_2. Therefore, the variations of major elements in the Mingxi lavas are probably due to the heterogeneous source lithology, rather than crystal fractionation.

The low-MgO suites (Zhangzhou and Zhanjiang) display high SiO_2 and Al_2O_3, and low $Fe_2O_3^T$ and Ni abundances, suggesting early fractionation from a more primitive parent melt (Brenna *et al.*, 2012*a*). The most primitive sample 17ZJ16-2 with the highest MgO (8·5 wt%) and Ni abundance (226 ppm) was chosen as the starting material to model crystal fractionation using PETROLOG 3. The variations of Cr, CaO and CaO/Al_2O_3 against MgO in the Zhanjiang lavas roughly form two trends. The positive trend points to some degree of clinopyroxene crystallization, whereas the Cr, CaO and CaO/Al_2O_3 values remain relatively constant as MgO decreases, and fall on the modeling trend of olivine fractionation (Fig. 5e, g and h). However, the weakly positive correlation between Ni and MgO suggests a very low degree of olivine fractionation (Fig. 5d), as Ni is highly compatible in olivine ($D_{Ni}^{Ol/melt} > 7$) (Kinzler *et al.*, 1990). In particular, the Zhangzhou lavas display scattered variations in CaO, $Fe_2O_3^T$ and TiO_2 as MgO decreases. This feature, together with the small variations in Ni and Cr abundances and CaO/Al_2O_3 ratios, cannot be explained solely by crystal fractionation processes, but is more likely to be controlled by a heterogeneous magma origin.

Among all the samples studied here, the increases in Al_2O_3 and SiO_2 with falling MgO (Fig. 5a and b) indicate very little fractionation of plagioclase, in agreement with the absence of depletion of Sr, Ba and Eu in the primitive mantle-normalized multi-element diagrams (Fig. 6).

In short, on the basis of Harker diagrams, the Fuding lavas have experienced olivine and clinopyroxene fractionation in stages during magma evolution, and the Zhanjiang samples have experienced clinopyroxene fractionation and a small degree of olivine fractionation. Fractional crystallization has little effect on the compositions of the high-MgO lavas (>10 wt%) from Fuding and Mingxi, and they are therefore closest to the primary magma. To further minimize the effect of fractional crystallization on the whole-rock compositions, we quantitatively calculated the potential primary magma compositions by addition of equilibrium olivine

(Supplementary Data Table S9). The detailed discussion of this will follow in a subsequent section on the lithology of mantle sources.

Spatial isotopic variations

Isotope compositions differ systematically among volcanoes of the outer and the inner belts. Except for the Zhanjiang lavas, which show large variations in Sr-, Nd- and Pb-isotope compositions, the lavas in Mingxi along the interior fault have the highest $^{143}Nd/^{144}Nd$ ratios (average value = 0·51291, n = 17) and the lowest $^{206}Pb/^{204}Pb$ ratios (average value = 18·29, n = 17), whereas the lavas in Jieyang, Fuding and Zhangzhou, located along faults closer to the coastline, have lower $^{143}Nd/^{144}Nd$ and higher $^{206}Pb/^{204}Pb$ ratios (Fig. 10). All the lavas of SE China, except those at Zhanjiang (the closest to Hainan Island), show a spatial increase in $^{143}Nd/^{144}Nd$ ratios and decrease in $^{206}Pb/^{204}Pb$ and $^{87}Sr/^{86}Sr$ ratios with distance from the Pacific trench.

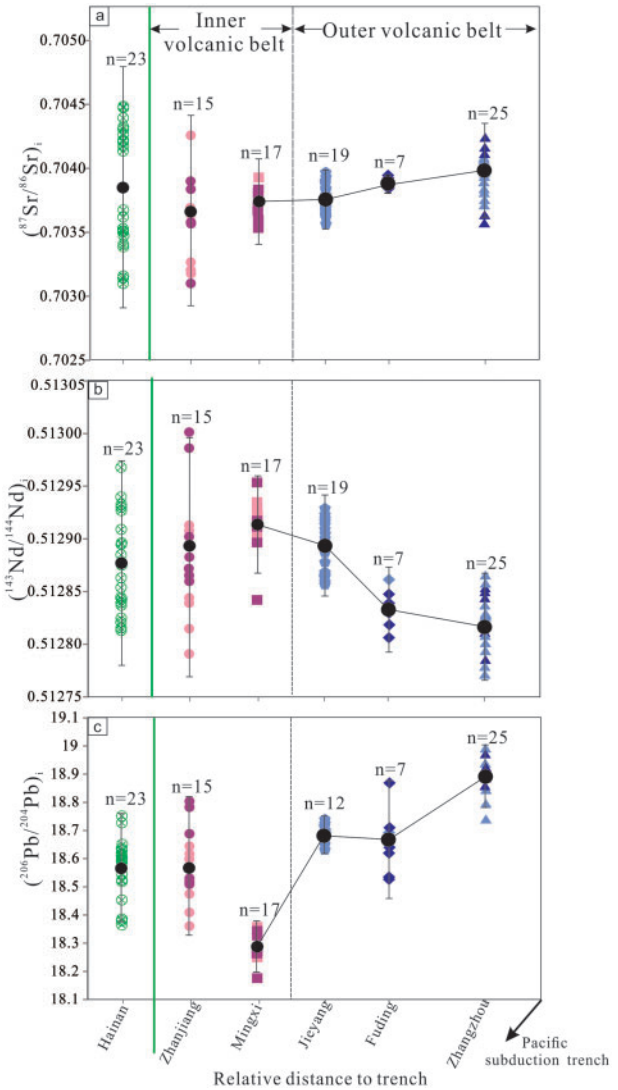

Fig. 10. Initial Sr, Nd and Pb isotopic variations of the Cenozoic basaltic lavas in SE China with their relative perpendicular distance to the Pacific subduction trench. The sources of the compiled data are the same as in Fig. 7. The dark and light colored symbols denote data obtained by this study and previous studies, respectively. The black circles represent average isotopic ratios of basaltic lavas from each location, and the error bar is 2σ. The geographical position of samples is shown in Fig. 2a.

On a local scale, the eruption ages of the volcanoes within the outer belt vary widely (26 – 6 Ma) (Fig. 3). However, the overall Nd- and Pb-isotope compositions of the lavas show a discernible trend from coast to inland, irrespective of their eruption ages (Fig. 10b and c). For example, the lavas in Jieyang, which erupted at 6 and 20 Ma, have uniform isotope compositions. These lavas, together with the >22 Ma lavas in Fuding, display higher $^{143}Nd/^{144}Nd$ and lower $^{206}Pb/^{204}Pb$ values than the *c.* 16 Ma Zhangzhou lavas, which were erupted close to the coast. The youngest lavas, which occur in the inner belt, have Sr–Nd isotopic compositions that become increasing larger than those to the east, but the Pb isotope ratios of the Mingxi lavas are distinct from those of Zhanjiang (Fig. 10c). The various Sr-, Nd-, and Pb-isotope compositions of the Zhanjiang basalts resemble those of the Hainan lavas (Figs 7 and 10), and given their similar age and spatial proximity, the simplest explanation for the isotopic resemblance is contribution from a common source within the Hainan plume (Wang *et al.*, 2013). With increasing distance from Hainan, isotopic variations become smaller. This is interpreted as preferential sampling of melts from fusible end-member components, which melt at low temperatures in the peripheral regime of the plume (e.g. Lassiter *et al.*, 2000).

Sun *et al.* (2017) proposed that the spatial variations in the radiogenic isotopic compositions in the region were due to variable degrees of partial melting of a metasomatized sub-lithospheric mantle. However, the nature of the metasomatizing agent was not discussed in detail. Alternatively, the isotopic variations may have resulted from contributions of distinct, enriched components to the mantle source. In either case, it is crucial to recognize the enriched mantle components in the sources of the Cenozoic lavas in SE China.

Mantle source enrichment

The Cenozoic basalts in SE China exhibit enriched Sr–Nd–Pb isotope compositions that plot in or close to the field of EM2-type OIB (Fig. 7; Zindler & Hart, 1986). The overall near-linear correlation of Sr–Nd isotope compositions of the Cenozoic lavas suggests two-component mixing of depleted mantle and an EM2-type mantle (Fig. 7a).

In terms of radiogenic isotopes, both the normal asthenospheric mantle and the sub-continental lithospheric mantle (SCLM) are possible candidates for the depleted mantle end-member, because the ultramafic xenoliths found in the Cenozoic basaltic lavas from SE China show depleted radiogenic isotopic features (Fig. 7; Tatsumoto *et al.*, 1992; Qi *et al.*, 1995). The depletion of HREE relative to LREE in the SE China lavas (Fig. 6e–h) has been interpreted as indicative of low-

degree partial melting in the presence of residual garnet (e.g. Zou *et al.*, 2000; Wang *et al.*, 2012; Huang *et al.*, 2013; Sun *et al.*, 2017; Zeng *et al.*, 2017), as this mineral phase has partition coefficients of HREE $>$ 1 (e.g. Pertermann *et al.*, 2004). Given the spinel–garnet phase transition lies at 70 – 80 km depth (Robinson & Wood, 1998), the SE China basalts are most probably derived from the asthenospheric mantle, because the lithosphere–asthenosphere boundary (LAB) beneath the coastal areas in South China lies at *c.* 80 km depth (An & Shi, 2006), and *c.* 55 km depth below Hainan Island (Wu *et al.*, 2004).

Several studies advocated that the elevated LREE/HREE ratios in intraplate basalts could also be produced by melting of garnet-free sources (e.g. Scott *et al.*, 2016). One option is melting of spinel-bearing, lithospheric peridotite that has been metasomatized by melts or fluids with 'garnet signature'. Partial melts from such sources are expected to be enriched in highly incompatible trace elements (e.g. Rb, Ba, Th, U) as well as LREE, as found in some OIB-type alkaline basalts (Pilet *et al.*, 2008; Pilet, 2015; Scott *et al.*, 2016). These basalts are also characterized by prominent negative K-anomalies, because the hydrous components in a metasomatized mantle are commonly stored in amphibole and/or phlogopite (Denis *et al.*, 2015; Scott *et al.*, 2016). However, the basalts studied here do not show strong negative anomalies in K (Fig. 6a–d), we thus favor a scenario in which the high LREE/HREE in SE China basalts is caused by residual garnet in the asthenospheric source region. Although rare, some ultramafic xenoliths in Cenozoic basalts in SE China include garnet (Xu *et al.*, 2003).

Moreover, ultramafic xenoliths hosted in the Cenozoic basalts in SE China provide direct information on the lithospheric mantle. It has been demonstrated that the composition of SCLM is heterogeneous beneath SE China, as represented by the trace element compositions of the peridotite xenoliths in the Mingxi and Zhangzhou basalts (Xu *et al.*, 2000). On the primitive mantle-normalized trace-element diagrams, xenoliths in the Mingxi basalts show a strong depletion of Nb and Zr. In contrast, the xenoliths in the Zhangzhou basalts display depletion of only Nb, without obvious depletion of Zr (Xu *et al.*, 2000, 2003). However, both the basaltic lavas from both Mingxi and Zhangzhou are enriched in Nb, without obvious Zr anomalies, which is inconsistent with the features of their respective underlying SCLM (Fig. 11). Thus, the asthenospheric mantle, rather than the SCLM, produced the depleted isotopic end-member in the source of the SE China basalts.

In addition to the *in situ* SCLM, the subducted oceanic lithospheric mantle, which is ubiquitous in the convecting mantle (Byerly & Lassiter, 2014), could also contribute depleted components to the source. However, this would be difficult to distinguish from the normal depleted MORB mantle (DMM) through geochemical compositions and conventional isotopes, if mixed with enriched, recycled crustal materials. The

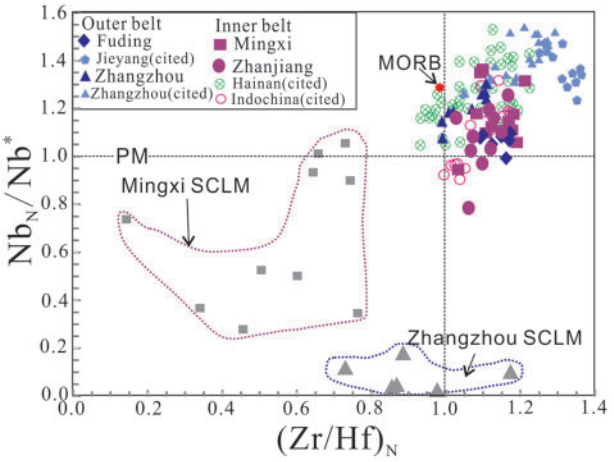

Fig. 11. Variations of Nb_N/Nb^* vs $(Zr/Hf)_N$ for the basaltic lavas from SE Asia, where Nb* is defined as $(Th_N^3 \times La_N^2)^{(1/5)}$, and subscript N denotes normalization to the values of the primitive mantle (McDonough & Sun, 1995). Values for MORB are from Hofmann (1988). The plotted data for peridotite xenoliths of the Mingxi and Zhangzhou basalts, representing the composition of the sub-continental lithospheric mantle (SCLM) beneath the sampled regions, are from Xu *et al.* (2000, 2003). The cited data for the SE Asian basalts can be found in Supplementary Data Table S8.

distinct recycled signatures of the subducted lithospheric mantle might be preserved in their Hf–Os isotope systematics (Bizimis *et al.*, 2007). Here, we use the DMM, which was relatively well constrained as the composition of the asthenospheric mantle (Workman & Hart, 2005), in the following trace element and isotopic modeling.

The origin of an EM2-type mantle reservoir remains a subject of debate. Among the great diversity of models, those most invoked are (1) recycled continental crust (Stracke *et al.*, 2003, 2005), (2) metasomatized SCLM (Niu & O'Hara, 2003), and (3) recycled oceanic crust plus sediments (Li *et al.*, 2015, 2016).

The lower continental crust, composed of eclogite or granulite of a higher density than peridotite, enters the convective upper mantle as an enriched mantle reservoir (Willbold & Stracke, 2006, 2010). However, geochemical studies of granulite or pyroxenite xenoliths hosted in Cenozoic basalts in SE China have shown that although the LCC is enriched in Sr and Nd isotopes ($^{87}Sr/^{86}Sr$ = 0·709816 ± 0·008061, $^{143}Nd/^{144}Nd$ = 0·511636 ± 0·000405, average value ± 1SD, n = 32), the xenoliths generally have unradiogenic Pb isotopic compositions (Liu *et al.*, 2004; Ying *et al.*, 2010; Huang *et al.*, 2013). The $^{206}Pb/^{204}Pb$ ratios of the LCC beneath SE China (16·52 ± 1·06, average value ± 1SD, n = 37) are obviously far lower than those of the lavas investigated in this study (18·59 ± 0·24, n = 26). In addition, the LCC typically has positive Pb and negative Nb and Ta anomalies in primitive mantle-normalized multi-element plots (Fig. 6; Rudnick & Gao, 2003), which is not consistent with the lavas studied here. Thus, it would be very difficult to produce the SE China basalts from a mantle source with a significant LCC component.

As an alternative to the LCC, we have investigated the possible role of metasomatized SCLM, a source commonly cited for enrichment of incompatible elements in OIB-like basalts (Niu & O'Hara, 2003). Metasomatized SCLM has also been invoked as an enriched component to explain the trace element signatures of the Cenozoic basaltic lavas in SE China (Ho *et al.*, 2003; Sun *et al.*, 2017), and this suggestion is supported by studies of mantle xenoliths in the Cenozoic basalts, showing that the SCLM beneath SE China has been widely metasomatized (Xu *et al.*, 2003). However, the Sr-, Nd- and Pb-isotope compositions of the peridotite xenoliths are too depleted (Tatsumoto *et al.*, 1992; Qi *et al.*, 1995) to generate an enriched mantle source for the basalts investigated in the current study (Fig. 7).

In summary, no evidence has been found in the LCC or SCLM that can account for the isotopic and trace element signatures of the basaltic lavas in SE China.

Recycling of oceanic crust plus sediments by subduction has been proposed to explain the enriched Sr–Nd isotope signatures and radiogenic Pb isotopes in EM2 mantle sources (Jackson *et al.*, 2007). Additionally, the involvement of terrigenous sediments originating from the UCC could also explain the high abundances of incompatible trace elements as well as some typical trace element ratios (e.g. low Ce/Pb and high Th/Nb) in EM-type OIBs (Stracke, 2012). As shown in Fig. 7a, both ancient and young recycled crustal materials (igneous crust plus overlying sediment) have high $^{87}Sr/^{86}Sr$ and low $^{143}Nd/^{144}Nd$ ratios. Thus, they could both potentially contribute to the enriched end-member needed to mix with a DMM source to account for the Sr–Nd isotope signatures in the lavas of SE China. Furthermore, in contrast to the LCC and metasomatized SCLM models discussed above, oceanic crustal recycling provides a good explanation for the radiogenic Pb-isotope compositions of the studied lavas.

Ancient dehydrated oceanic crust with high U/Pb ratios would produce a mantle reservoir with high Pb-isotope compositions owing to its long-term evolution, and such material was proposed to explain the highly radiogenic Pb isotopic compositions of HIMU lavas (e.g. Hanyu *et al.*, 2014). The correlation between $^{206}Pb/^{204}Pb$ and $^{207}Pb/^{204}Pb$ ratios can potentially give important information for the recycling ages of the geochemical reservoir, because both ratios evolve concurrently depending on the U/Pb ratios in the mantle source. The non-linear correlation between $^{207}Pb/^{204}Pb$ and $^{206}Pb/^{204}Pb$ in all the analyzed samples (Fig. 7b) cannot be explained by either a simple binary mixing model or a single 'mantle isochron', and most probably reflects the presence of recycled oceanic crust with various ages in the source. As shown in Fig. 7d, the $^{207}Pb/^{204}Pb$ values at a given range of $^{206}Pb/^{204}Pb$ ratios in the lavas broadly straddle the calculated isopleths.

The ages of recycled slabs will be discussed in more detail below. Beforehand, however, the potential components of the recycled materials need to be evaluated, because the varied isotopic parent–daughter ratios will vary depending on the slab origin; for example, MORB, gabbro, and both pelagic and detrital sediments (Sobolev *et al.*, 2011). In the following, we first discuss the lithology of the geochemically enriched end-member components, and then their origins and the mechanisms by which these materials were delivered to the melting region beneath SE China.

Nature and components of recycled oceanic crust materials in the source

Lithology of mantle sources

The oceanic crust enters the peridotitic mantle by subduction, and then is preserved in the deep mantle as an isolated mafic eclogite or garnet-pyroxenite domain (e.g. Sobolev *et al.*, 2007). Isotopes combined with special trace element features are helpful to recognize the signals of recycled crust in mantle source, but cannot distinguish whether the crust is present as a lithological unit in the source, or whether only the geochemical signal of the recycled crust was imprinted into the peridotite (Herzberg, 2011). The whole-rock major oxides of basaltic lavas can be used to evaluate the lithology of the source rocks.

To assess source lithology for the volcanic rocks, the least differentiated samples are selected. As mentioned previously, a decrease of CaO at MgO $<$ 9 wt% is probably due to clinopyroxene crystallization (Herzberg & Asimow, 2008). Thus, samples with MgO $\geq$ 9 wt% and CaO $>$ 8 wt% were chosen as starting materials for the calculation of their primary magmas. Olivine in equilibrium with melt was incrementally added until the melt equilibrated with mantle olivine at $Fo_{90.7}$, which is the most magnesian olivine found in the SE China basalts (Wang *et al.*, 2012; Liu *et al.*, 2015; Zeng *et al.*, 2017). The calculated results are shown in Supplementary Data Table S9. The primary magma compositions of the samples studied here are not compromised by deep augite crystallization, which lowers CaO only when the primary magma evolved by olivine fractionation to about 7·5 wt% MgO (the black dashed arrow shown in Fig. 12a; Herzberg, 2006). Also in Fig. 12, primary magmas derived from fertile peridotite have minor variations in CaO contents at a given MgO value, and lavas with CaO contents lower than those defined by the green line are potential pyroxenite partial melts (Herzberg & Asimow, 2008). The various CaO contents (6·5 – 10·5 wt%) of the calculated primary melts suggest that their source material was heterogeneous. Most of the calculated primary magmas of the studied lavas plot in the field of pyroxenite partial melts (Fig. 12a).

The involvement of mafic lithologies in the genesis of the studied rocks is also suggested by TiO_2 contents (1 – 3 wt%) and Fe/Mn ratios of the estimated primary melts. Abundances of TiO_2 are greater than experimental melts derived from peridotites ($<$2 wt%; e.g. Tuff *et al.*, 2005) and are consistent with those from a mixture of peridotite and basalt (Fig. 12b). Higher Fe/Mn ratio is also diagnostic of melts from mafic lithologies

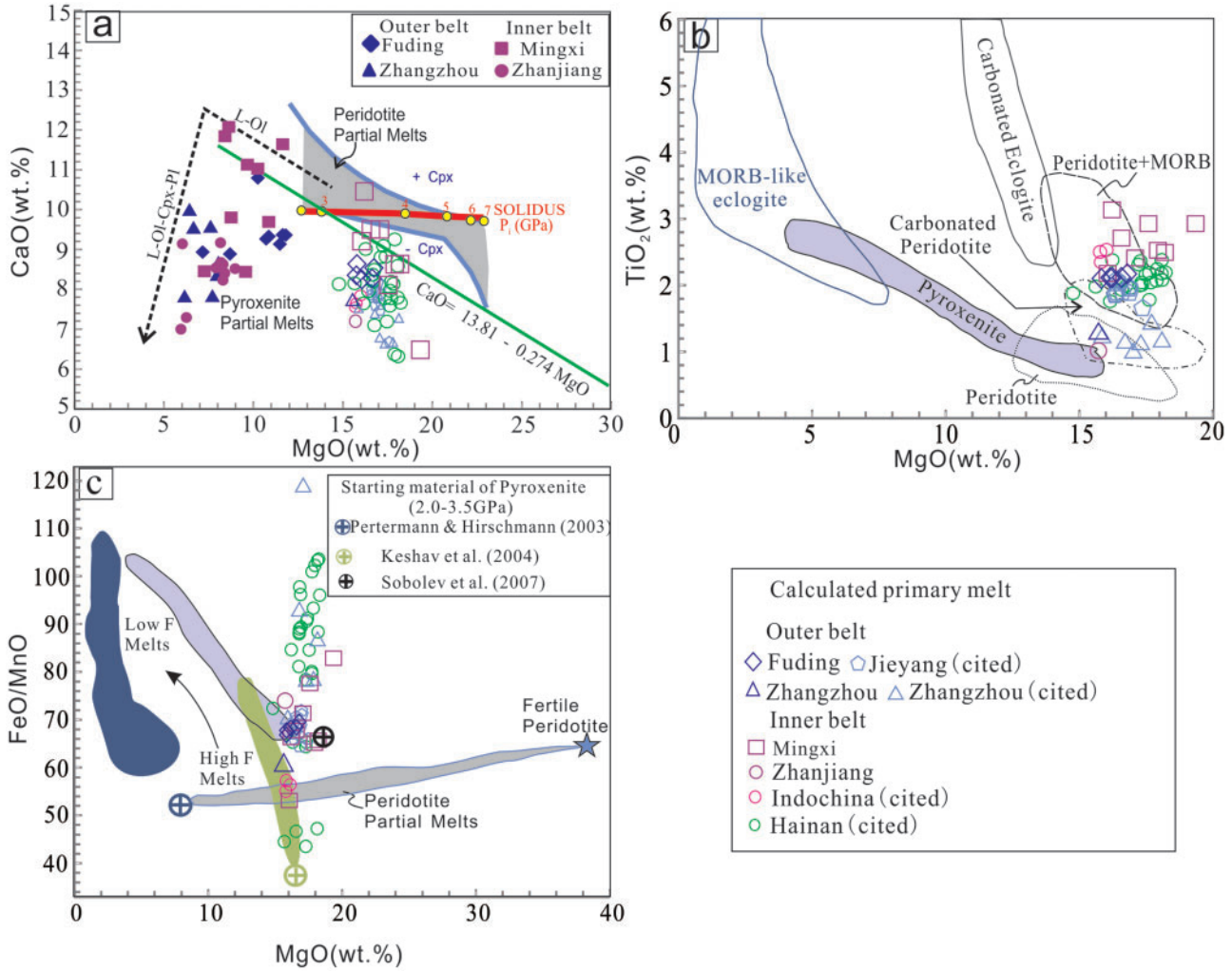

Fig. 12. Variations of (a) CaO vs MgO, (b) TiO_2 vs MgO, and (c) FeO/MnO vs MgO for the calculated primary magmas of the basaltic lavas from SE Asia (open symbols). Samples with high MgO (≥9 wt%) and high CaO (>8 wt%) are selected as starting components to calculate the primary magma by adding equilibrium olivine, until the melts are in equilibrium with an olivine composition of $Fo_{90.7}$ (assuming that 10 % of the total iron is Fe^{3+}, and assuming a constant $(Fe^{2+}/Mg)_{olivine}/(Fe^{2+}/Mg)_{melt} = 0.3$; Roeder & Emslie, 1970). The calculated results are shown in Supplementary Data Table S9. The original CaO and MgO contents of SE China basalts are also plotted for comparison, as shown by filled symbols in (a). Peridotite and pyroxenite partial melt fields separated by the thick green line in (a) are after Herzberg & Asimow (2008). The black dashed line with an arrow in (a) represents the fractionation of a crystal assemblage of olivine + clinopyroxe + plagioclase from the peridotitic primary magma, and L denotes liquid. The sources of data for high-pressure experimental partial melts of mantle rocks shown in (b) are as follows: MORB-like eclogite: 2·0–3·0 GPa, G2 (Pertermann & Hirschmann, 2003); Pyroxenite: 3·5 GPa, Px-1 (Sobolev *et al.*, 2007); Carbonated Eclogite: 3·0 GPa, SLEC1 + 5·0 wt% CO_2 (Dasgupta *et al.*, 2006); Peridotite: 2·5–3·0 GPa, HK-66 and KLB-1 (Hirose & Kushiro, 1993); Peridotite + MORB: 3·0 GPa, KLB-1 + MORB (Kogiso *et al.*, 1998); Carbonated Peridotite: 3.0 GPa, KLB-1 + 1.0 wt% CO_2 (Dasgupta *et al.*, 2007). The experimental partial melts of pyroxenites and peridotites in (c) show the different effects of the melt fraction on FeO/MnO. Primary magmas derived from partial melting of fertile peridotite are from Herzberg (2006).

because of the higher compatibility of Mn ($D_{Mn}^{Cpx/melt} = 1.11$) over Fe ($D_{Fe}^{Cpx/melt} = 0.71$) in cpx (Le Roux *et al.*, 2011). The Fe/Mn ratios in the primary melts (65·7 ± 6·8) are significantly higher than those of primitive MORB (54·0 ± 1·2; Qin & Humayun, 2008), implying the involvement of a pyroxenite source. When compared with experimentally derived partial melts from pyroxenite and peridotite, the calculated primary melts show FeO/MnO ratios that vary significantly at a relatively constant MgO content, which resembles the features of pyroxenite partial melts (Fig. 12c; Pertermann & Hirschmann, 2003; Keshav et al., 2004), and this supports the contribution of pyroxenite as a source lithology. In addition, olivine phenocrysts in the Hainan basalts have comparably low CaO and high Ni and Fe/Mn to those in Hawaiian basalts (Liu *et al.*, 2015), which have been interpreted as the partial melts of pyroxenites (Sobolev *et al.*, 2005, 2007), providing further evidence for contributions of pyroxenite in the source.

To further constrain the lithology of mafic components, calculated compositions of primary magmas are projected onto the normative Olivine–Quartz–Calcium Tschermak's (CATS) plane, and compared with cotectic boundaries under variable pressures (3–6 GPa) in

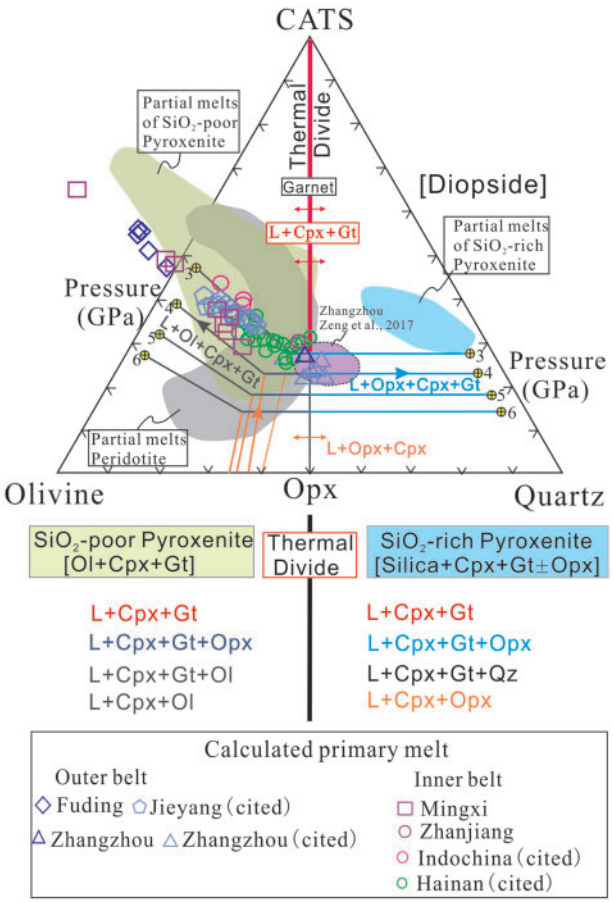

Fig. 13. Projections (mol%) of calculated primary magma compositions for the SE Asian basalts from or towards Diopside into the plane Olivine–Quartz–Calcium Tschermak's (CATS). The cotectics of [L + Opx + Cpx + Gt] and [L + Ol + Cpx + Gt] at pressure from 3 to 6 GPa are from Herzberg (2011). The thick red line denotes the pyroxene–garnet plane (thermal divide), which is used to identify high- and low-SiO_2 pyroxenites on the SiO_2-rich and -poor sides, respectively. The projection code is from Herzberg (2011). Experimental partial melts of SiO_2-rich and -poor pyroxenite (Herzberg, 2011, and references therein) and peridotite (Walter, 1998; Grove *et al.*, 2013) are projected for comparison. Also shown are the primary magmas for the Zhangzhou lavas estimated by Zeng *et al.* (2017), in which the basaltic samples that experienced only olivine fractionation (although MgO < 9 wt%) were corrected to be in equilibrium with an olivine composition of Fo_{90}. L, liquid; Ol, olivine; Gt, garnet; Cpx, clinopyroxene; Opx, orthopyroxene; Qz, quartz.

melting experiments (Fig. 13; Herzberg, 2006, 2011). Most of the estimated primary magma compositions of SE China basalts plot in the SiO_2-poor side of the pyroxene–garnet plane (thermal divide), and lie on the cotectic boundaries between 3 and 4 GPa. At this condition, melts are in equilibrium with the assemblage of olivine + clinopyroxene + garnet, consistent with the inference that there are garnet-bearing mafic lithologies present in the source region (e.g. silica-deficient pyroxenite). It has been demonstrated that the melts derived from a SiO_2-poor assemblage can mix freely with those of peridotite in the melting region (Herzberg, 2011). A study of melt inclusions in olivine of the Hainan basalts supports the inference that peridotitic and pyroxenitic magma mixing occurs at depth. It was found that subalkaline and alkaline basaltic melt inclusions co-occurred in a single sample (Liu *et al.*, 2015).

The strongly alkaline basanites from Fuding and Mingxi are nepheline normative, and thus plot outside the CATS plane. It is noted that these samples plot on the extension of the olivine–clinopyroxene–garnet cotectic boundary at 3 GPa, suggesting that they are melting products of a more silica-deficient mafic lithology than the mildly alkaline basalts in SE China. Alternatively, partial melting of peridotite and/or pyroxenite at high pressures in the presence of CO_2 could generate strongly silica-undersaturated alkaline magmas (Dasgupta & Hirschmann, 2006; Dasgupta *et al.*, 2007, 2010), and could contribute to shifting the melt compositions to the SiO_2-poor side of the thermal divide (Herzberg, 2011). Here, we hold the view that carbonated components could play a role in the source of ultra-alkaline basalts in SE China, which is consistent with the inferences drawn by Zeng *et al.* (2017).

In short, major element compositions of the primary magmas in SE China are best reconciled with melting of mafic lithologies admixed with the peridotitic mantle. In the following section, we discuss the protoliths of the mafic lithologies mainly based on trace-element characteristics.

Chemical evidence for dehydrated oceanic crust

All studied basalts display an enrichment in Nb and Ta relative to Th, U, and LREE in the primitive mantle-normalized trace element diagram (Fig. 6a–d), with high values of $Nb_N/Nb^* \geq 1$ (Fig. 14a; see figure caption for a definition of Nb*). In addition, most of the basalts show negative anomalies of Pb relative to Ce and Pr, with low values of $Pb_N/Pb^* \leq 1$ (Fig. 14a; see figure caption for a definition of Pb*). Niobium and tantalum are fluid-immobile elements and are preferentially retained in the oceanic crust during dehydration in the subduction zone, whereas K, Li, Pb and LILE are fluid-mobile elements and are transferred extensively to the overlying mantle wedge (e.g. Elliott *et al.*, 1997; Kessel *et al.*, 2005). Consequently, a residual oceanic slab, metamorphosed to eclogite, exhibits enrichment of Nb and Ta and depletion of Pb, features that are consistent with the observed signatures of the studied lavas in SE China. The LILE are also anticipated to show depletion, although the lavas in SE China do not show such features. We infer that the magma source would be fertilized in these elements by addition of sediments before subduction into the mantle (discussed below). Among all the basaltic lavas in SE Asia, those from Indochina, Hainan Island and Zhanjiang have higher Pb_N/Pb^* values at a given Nb_N/Nb^* value and slightly positive K anomalies (Figs 6 and 14), implying that their source materials experienced less dehydration during subduction than those in other localities. Similarly, the generally negative correlation between $(Ce/Pb)_N$ and $(Li/Y)_N$ indicates that the source materials of the Zhangzhou

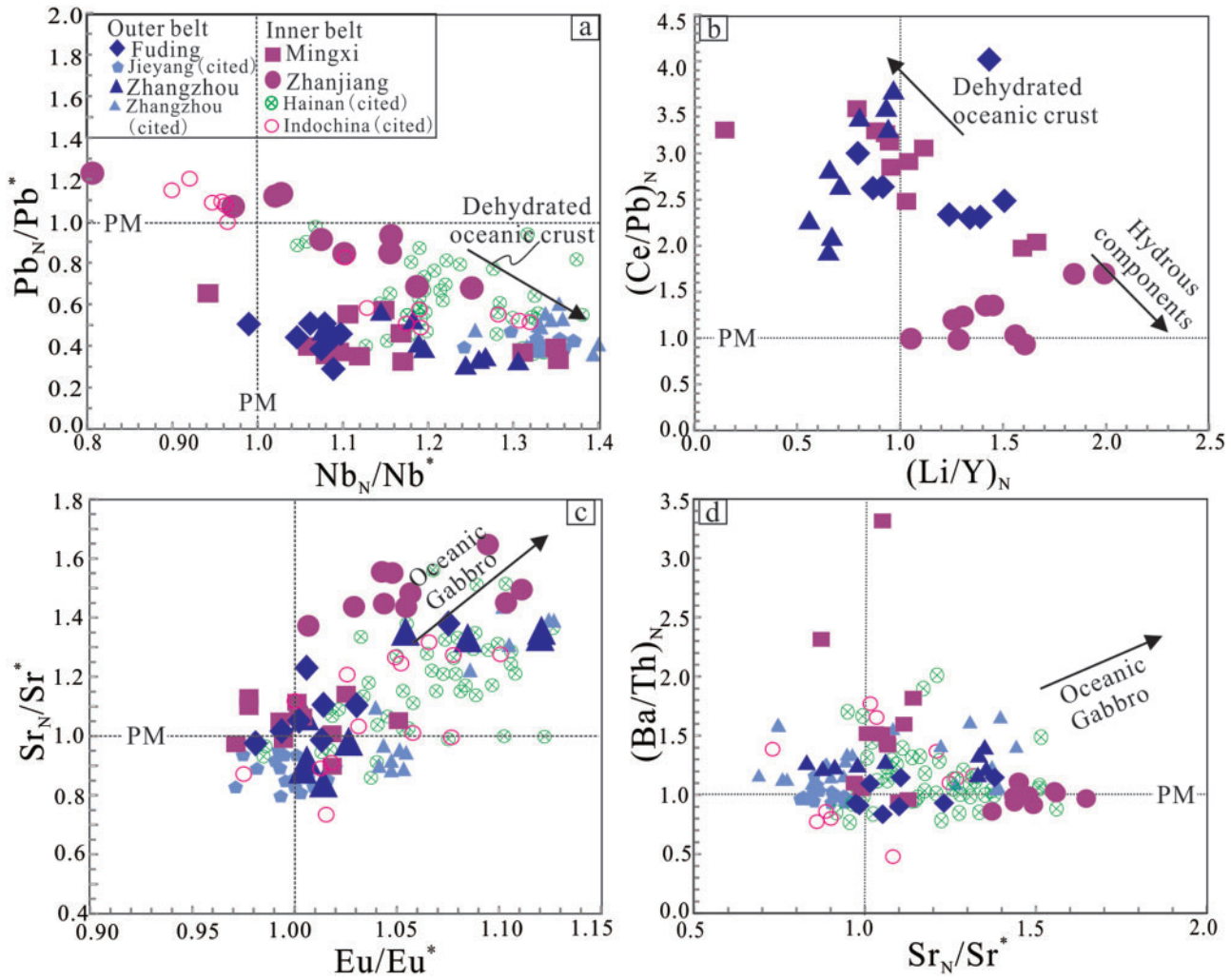

Fig. 14. Variations of (a) Pb_N/Pb^* vs Nb_N/Nb^*, where Pb* is defined as $(Ce_N \times Pr_N)^{(1/2)}$, and Nb* is defined as $(Th_N^3 \times La_N^2)^{(1/5)}$; (b) $(Ce/Pb)_N$ vs $(Li/Y)_N$; (c) Sr_N/Sr^* vs Eu/Eu*, where Sr* is defined as $(Pr_N^2 \times Nd_N)^{(1/3)}$, and (d) $(Ba/Th)_N$ vs Sr_N/Sr^*. Subscript N denotes normalization to the values of the primitive mantle (McDonough & Sun, 1995). Eu* is defined as the interpolation between Sm and Gd concentrations on a REE diagram (Fig. 6e–h), and $Eu/Eu^* = Eu/(Sm \times Gd)^{(1/2)}$, where Eu, Sm and Gd are normalized to chondrite values (Sun & McDonough, 1989). The source of the compiled data can be found in Supplementary Data Table S8.

lavas have undergone a more intensive dehydration process, and the source materials of the Zhanjiang lavas are slightly more hydrous than the others (Fig. 14b).

The enrichments of Ba and Sr, resulting in high $(Ba/Th)_N$, and Sr_N/Sr^* ratios (Fig. 14c–d; see figure caption for a definition of Sr*) are contrary to the inference that mafic lithology in the source of SE China basalts is derived from dehydrated oceanic slab (Kogiso *et al.*, 1997; Kessel *et al.*, 2005). Because Ba and Sr are incompatible in most of the mafic minerals, but are compatible in plagioclase, previous studies suggested that the elevated Ba/Th and Sr_N/Sr^* ratios of some intraplate basalts (e.g. Hawaiian basalts and Logudoro basalts) could be attributed to melting of plagioclase-rich gabbro ($D_{Ba}^{plagioclase/melt} > D_{Th}^{plagioclase/melt}$; Hofmann & Jochum, 1996; Gasperini *et al.*, 2000). A plagioclase-rich source should also be characterized by a positive Eu anomaly relative to its neighboring elements Sm and Gd (Pietruszka *et al.*, 2013). The overall positive correlation of Sr_N/Sr^* and Eu/Eu* [$Eu/(Sm \times Gd)^{(1/2)}$; all normalized to chondrite values] in SE China basalts (Fig. 14c) suggests the presence of a plagioclase-rich component in the source.

In general, there are two potentially plagioclase-rich domains in the mantle: (1) gabbroic lower oceanic crust (now eclogite or pyroxenite; Hofmann & Jochum, 1996); (2) lower continental crust rocks (e.g. felsic granulite; Liu *et al.*, 2008). The possibility of LCC in the source of the SE Asia lavas has been ruled out based on the Pb isotopes as discussed above. We contend that the presence of recycled oceanic gabbro, which entered the source region as part of the subducted crust, accounts for the observed high values of Sr_N/Sr^* (>1),

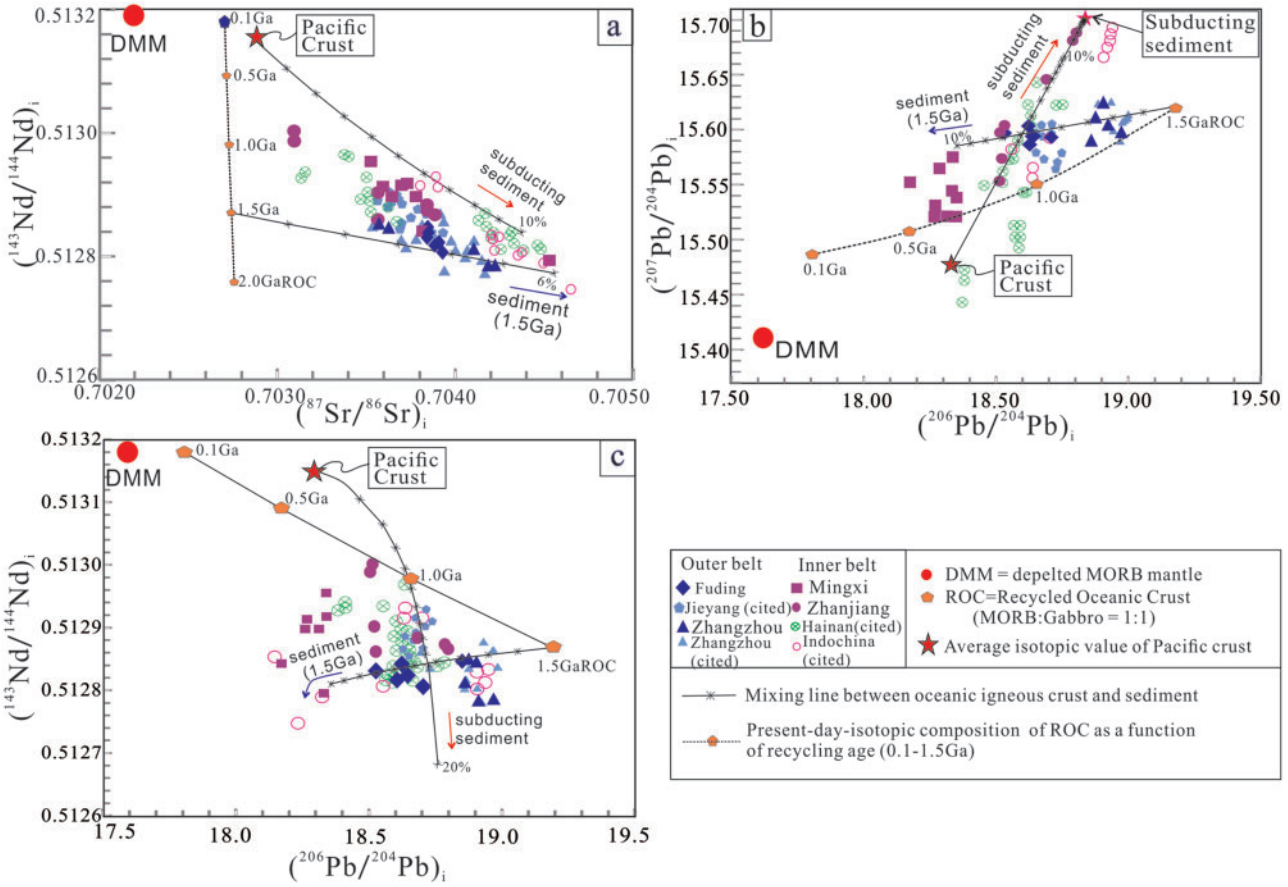

Fig. 15. (a) $(^{143}Nd/^{144}Nd)_i$ vs $(^{87}Sr/^{86}Sr)_i$, (b) $(^{207}Pb/^{204}Pb)_i$ vs $(^{206}Pb/^{204}Pb)_i$, and (c) $(^{143}Nd/^{144}Nd)_i$ vs $(^{206}Pb/^{204}Pb)_i$ of basaltic lavas from SE Asia. This figure shows the Sr–Nd–Pb isotopic evolution of the recycled oceanic crust, and the effect of sediment input on the isotopic composition of bulk subducted materials. Additionally, it is used to explain the mixing of end-members selected in Fig. 7. Dashed lines with orange pentagons denote the calculated present-day-isotopic compositions of a dehydrated recycled oceanic crust (ROC) consisting of 50% MORB and 50% gabbro as a function of recycling age (0·1 – 1·5 Ga). Detailed information relating to the isotopic evolution of the recycled oceanic crust can be found in the main text and Supplementary Data Table S5. Continuous lines denote the mixing curves between the recycled igneous crust and sediments.

Eu/Eu* (>1) and $(Ba/Th)_N$ in the basaltic lavas (Fig. 14c and d). The extents of the Sr and Eu anomalies in the lavas could depend on the relative amounts of plagioclase in the gabbroic materials of their sources.

Involvement of sediments

Recycled sediments have been widely suggested as a source of the enriched geochemical features of intraplate basaltic rocks (Huang & Frey, 2005; Kuritani *et al.*, 2011). Recently, evidence accumulated from Mg isotope studies indicates the presence of carbonated subducted sediments in the source of the Cenozoic basalts in East China (e.g. Wang *et al.*, 2017, 2018).

Owing to the high abundances of incompatible trace elements in sediments, the addition of small amounts of sediments will result in a considerable impact on trace-element (e.g. Cs, Rb, Ba, Th, U, La and Pb) and isotopic composition of the bulk subducted materials (Plank & Langmuir, 1998; Stracke *et al.*, 2003). Subducting sediments possess higher time-integrated $^{87}Sr/^{86}Sr$ and $^{207}Pb/^{204}Pb$, and lower $^{143}Nd/^{144}Nd$ ratios than the igneous Pacific crust (Fig. 15; e.g. Huang *et al.*, 2005). Some lavas from Zhanjiang and Indochina regions have conspicuously high $^{207}Pb/^{204}Pb$ ratios, plotting in the area defined by subducting sediments in the Mariana Trench (Fig. 7b; Plank & Langmuir, 1998). Together with the Mingxi lavas, the inner belt lavas (Zhanjiang and Mingxi) form a broad near-linear array on a $^{207}Pb/^{204}Pb$–$^{206}Pb/^{204}Pb$ plot, pointing toward the composition of DMM and subducted Pacific crust with some amount of sediments (Fig. 7b). The Pb isotopes in Zhanjiang basalts are largely contributed from subducted Pacific materials, and a decreasing contribution of subducted materials is suggested for the Mingxi lavas with relatively low $^{206}Pb/^{204}Pb$ ratios. Inclusion of subducted Pacific plate material in the matrix peridotitic mantle formed a hybrid lithology, and acquired time-integrated isotopic compositions in the mantle source of lavas from the inner volcanic belt in SE China, Hainan Island and the Indochina peninsula. This inference is further supported by the overall positive correlation of $(Th/Nb)_N$ and $^{207}Pb/^{204}Pb$ ratios in the inner belt lavas, as well as in the Hainan and Indochina lavas (Fig. 16). The addition of sediments to the igneous oceanic crust

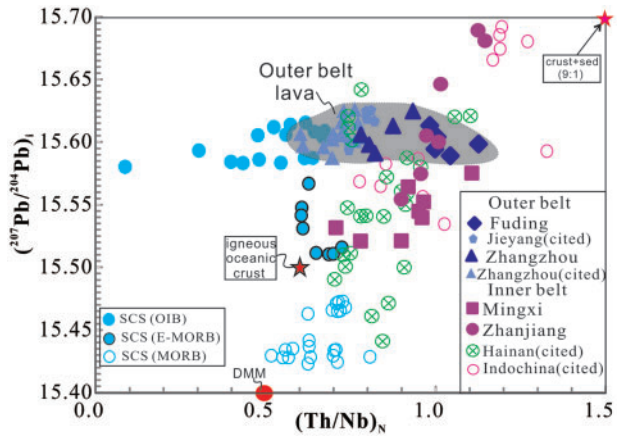

Fig. 16. Variation in $(^{207}Pb/^{204}Pb)_i$ vs $(Th/Nb)_N$ for the basaltic lavas from SE Asia. Th and Nb abundances are normalized to the values of primitive mantle (McDonough & Sun, 1995). The reference values of the end-members are as follows. DMM: $(Th/Nb)_N = 0{\cdot}5$, $^{207}Pb/^{204}Pb = 15{\cdot}4$ (Workman & Hart, 2005); igneous oceanic crust: $(Th/Nb)_N = 0{\cdot}6$, $^{207}Pb/^{204}Pb = 15{\cdot}5$ (Stracke *et al.*, 2003); sediment (GLOSS): $(Th/Nb)_N = 10$, $^{207}Pb/^{204}Pb = 15{\cdot}8$ (Plank & Langmuir, 1998). The compiled sources of the data can be found in Supplementary Data Table S8. The abbreviation crust + sed denote igneous oceanic crust plus sediments.

would increase Th/Nb ratios in the bulk subducted materials owing to the strong depletion of Nb in sediments. Therefore, the increase in Th/Nb ratios with increasing $^{207}Pb/^{204}Pb$ is attributed to sediment input in the hybrid source.

It is noted that, compared with the inner belt rocks, the outer belt lavas (Fuding and Zhangzhou) display a rather limited variation in $^{207}Pb/^{204}Pb$ ratios whereas their $(Th/Nb)_N$ ratios vary (Fig. 16). Moreover, the overall array formed by the outer belt lavas in the $^{206}Pb/^{204}Pb$ vs $^{207}Pb/^{204}Pb$ plot points toward a composition different from that of modern sediments (Fig. 15b). At a given $^{87}Sr/^{86}Sr$ ratio, these rocks have lower $^{143}Nd/^{144}Nd$ ratios than the inner belt rocks (Fig. 7a), which are shifted to the area below the mixing array formed by DMM and Pacific oceanic materials. This suggests the involvement of an end-member component that differs from modern sediments. We speculate that this end-member component is derived from an ancient subducted slab, which possesses high time-integrated Pb isotopic compositions. The feasibility of this scenario is examined in the following section.

Recycling age of the subducted oceanic crust in the source region

In this section, we consider the formation or recycling age of the ancient oceanic materials preserved in the source of the outer belt rocks, and then clarify the effect of various-aged oceanic materials on the isotopic heterogeneity of the Cenozoic SE China basalts.

In the $^{207}Pb/^{204}Pb$–$^{206}Pb/^{204}Pb$ plot (Fig. 15b), the lavas within the outer volcanic belt fall on the higher $^{206}Pb/^{204}Pb$ side of the array formed by mean compositions of Pacific oceanic crust and sediments. This suggests the involvement of a reservoir with time-integrated higher μ ($^{238}U/^{204}Pb$) and κ ($^{232}Th/^{238}U$) values relative to the subducted Pacific crust in the source of the outer zone basalts. We suggest that the Pb isotope arrays formed by the lavas from individual localities are not isochrons, but mixing trends; thereby the slope of the arrays does not directly relate to the reservoir formation ages.

To constrain the formation or recycling ages of magma sources, we apply forward modeling for isotope evolution of subducted lithologies. The model assumes that subducted materials consist of basaltic crust (recycled oceanic crust; ROC) and surface sediment. A two-stage Pb evolution model proposed by Stracke *et al.* (2003) was employed to calculate the present-day Pb isotopic ratios of the ROC as function of recycling ages (Fig. 15b). We estimated an average composition of ROC as a mixture of basalt and gabbro (ROC = 50 % N-MORB + 50 % gabbro). Modification of parent/daughter element ratios during subduction was evaluated on the basis of element mobility obtained in dehydration experiments (Kogiso *et al.*, 1997; Kessel *et al.*, 2005; Tsay *et al.*, 2017). Details about the specific parameters used in our calculations are given in Supplementary Tables S4 and S5.

The Pb isotope evolution of ROC is calculated based on the following assumptions: the onset time of Pb isotope evolution is 4·55 Ga with terrestrial $\mu_i = 8{\cdot}2$ (first stage), and the μ (as well as κ) change at the time of subduction (second stage). The model employs variable ages from 0·1 to 1·5 Ga as the onset of the second stage. The first stage between 4·55 Ga and the formation time of the oceanic crust corresponds to the evolution of an oceanic crustal reservoir, and the second stage from the time of crust subduction to the present corresponds to the evolution of the ROC. Modeling shows that the Pb-isotopic signature of the Zhangzhou lavas matches well with the melts from 1·5 Ga dehydrated ROC with $\mu = 13{\cdot}8$. Using this age constraint, the Sr–Nd isotope evolution of the ROC was then calculated, yielding a low $^{143}Nd/^{144}Nd$ ratio consistent with the values observed in the outer belt rocks, but the $^{87}Sr/^{86}Sr$ ratio is significantly lower than those in the outer belt rocks (Fig. 15a). The discrepancy of the $^{87}Sr/^{86}Sr$ value between the calculated ROC and the outer belt rocks is due to the contribution of ancient sediment.

For evaluating the isotopic evolution of sediment, we assume that the sediments subducted together with the ROC. A three-stage Pb growth model is used to simulate the Pb evolution in recycled sediment. The first stage is from 4·55 to 3·7 Ga following Stacey & Kramers (1975). This stage is followed by a crustal history between 3·7 Ga and the time of sediment subduction. The third stage is from the time of sediment subduction to the present, corresponding to the evolution history of subducted sediments in the mantle as an isolated geochemical domain. Owing to the low U/Pb ratio in sediments (0·08 for global subducted sediments; Plank, 2014) compared with dehydrated oceanic crust (0·22; Stracke *et al.*, 2003), the inclusion of ancient sediments

in the recycled slab results in less radiogenic Pb isotopic compositions (Fig. 15b). As for Nd isotopes, the $^{147}Sm/^{144}Nd$ ratio of neither oceanic crust nor sediments is expected to change significantly during hydrothermal alteration or dehydration processes, compared with Rb/Sr, U/Pb and Th/U (Eisele *et al.*, 2002). The difference in concentration between average MORB (Hofmann, 1988) and average subducted sediment is small ($Nd_{sed}/Nd_{MORB} = 2{\cdot}4$). Thus, minor amounts of ancient sediments would not significantly change the $^{143}Nd/^{144}Nd$ ratio of the ROC through hybridization. The lavas from Zhangzhou and Fuding fall on the mixing line between 1·5 Ga ROC and sediment in the $^{207}Pb/^{204}Pb$–$^{206}Pb/^{204}Pb$ and $^{143}Nd/^{144}Nd$– $^{206}Pb/^{204}Pb$ space (Fig. 15b and c). The isotope variations in rocks within the outer volcanic belt may be due to the varying contributions of ancient sediments to the source.

The above lines, taken together, lead us to conclude that the hybrid lithology in the source of the outer belt lavas was formed by the inclusion of ancient recycled oceanic materials (1·5 Ga) in the matrix peridotite. We simulated the mixing relation between DMM and the ancient recycled materials using Sr–Nd–Pb isotopic variations (Fig. 7). Given that the recycled materials are more fusible and possess more enriched isotopic signatures than the DMM, the isotopic compositions of the outer belt lavas are heavily biased towards the enriched end-member. The difference in isotopic variations between the lavas from Fuding and Zhangzhou mainly derives from different proportions of sediment included in the recycled crust. The Fuding lavas contain a greater sediment component in the source, as indicated by lower radiogenic Pb isotopes than yielded by the Zhangzhou lavas (Fig. 7b and c).

As mentioned, the mantle beneath SE China contains fragments of subducted oceanic crust with various ages. The presence of young ROC is thought to be related to the continuing subduction of the Pacific plate, which is supported by the geophysical observations and the tectonic background; that is, the high-velocity seismic anomaly in the MTZ beneath East China (Huang & Zhao, 2006), and the high convergent velocity of the western Pacific plate towards the Eurasia plate (7 cm a^{-1}), which yields an age of the stagnant slab beneath SE China as young as *c.* 100 Ma (Hauff *et al.*, 2003; Liu *et al.*, 2017). Given the prolonged subduction of the (paleo-) Pacific plate (>160 Ma; Kimura *et al.*, 2018), the Pacific components may have played a dominant role in time-integrated isotopic features of late-stage volcanoes within the inner volcanic belt of SE China.

In summary, the spatial variations in Sr–Nd–Pb isotopic compositions of the late Cenozoic basalts in SE China from the coast to inland were caused by recycled oceanic crusts of various ages in the mantle source. An ancient recycled oceanic crust (1·5 Ga) was the dominant enriched domain in the source of the outer belt rocks, whereas the subducted (paleo-) Pacific slab (*c.* 100 Ma) was the major enriched source of the inner belt rocks.

Magmatic response to Pacific plate subduction and the Hainan plume

The Pacific plate has been subducting beneath the East Asian continent since the Mesozoic. Tectonic extension has occurred during this period, leading to the formation of continental marginal basins with deep faults and lithospheric thinning in East Asia (Su *et al.*, 2017 ; Xu *et al.*, 2019). The opening of the SCS and upwelling of the Hainan plume are also key factors in the tectonic evolution of East Asia (Yu *et al.*, 2018). However, the magmatism in response to these complex processes remains elusive. Here, we discuss the late Cenozoic tectono-magmatic response to subduction of the Pacific plate in SE Asia, which occurred in two stages, namely the opening of the SCS during the syn-spreading stage (*c.* 32 – 16 Ma) and then the post-spreading stage (<16 Ma).

Syn-spreading stage: initiation of the Hainan plume

Two alternative models have been proposed as main drivers of the SCS opening: (1) rollback of the Pacific slab (e.g. Niu, 2014, 2018); (2) upwelling of the Hainan plume (e.g. Chen *et al.*, 2017). As mentioned, the existence of the Hainan plume has been demonstrated by the findings of numerous studies; that is, the presence of a seismic anomaly extending into the lower mantle close to the core–mantle boundary (CMB; e.g. Zhao, 2007; Wei & Chen, 2016), large-scale surface uplift in southern Hainan Island from the Oligocene to *c.* 5 Ma (Shi *et al.*, 2011), and the anomalously higher potential mantle temperature than the surrounding mantle (Wang *et al.*, 2012, 2013). Lack of features typical of hotspot magmatism, such as a linear age progression in a volcanic chain (e.g. Hawaii) and huge volumes of lava succession (e.g. Emeishan), makes the existence of the Hainan plume controversial. More recently, geochemical studies show many similarities between the basaltic lavas in SE Asia and typical plume-related lavas, such as the hotter-than-normal temperature in the mantle beneath Vietnam, Hainan and the SCS (Wei & Chen, 2016; An *et al.*, 2017; Yang *et al.*, 2019). In the present study, geochemical signatures of various-aged ROC were found in the mafic lavas occurring in the regions around SE China. The ROC is most probably delivered by the Hainan mantle plume. The geographically related compositional heterogeneities in SE China basalts are difficult to explain simply by occasional asthenospheric upwellings, in which the enriched and depleted components are randomly distributed (Ho *et al.*, 2003). This in turn suggests that the compositional heterogeneities in these lavas must reflect the spatial geochemical distribution within a plume. In the subsequent sections, we will clarify the role of the Hainan plume in the origin of the basaltic lavas in SE Asia.

Different from the normal MORB derived from the depleted upper mantle, the ridge segments in the SCS include basalts with E-MORB-like trace element features

and enriched Sr–Nd–Pb isotopic compositions akin to those of the Hainan basalts (Fig. 7; Yu *et al.*, 2018; Zhang *et al.*, 2018). Within the SCS, normal MORB and OIB-type alkali basalts also occur. The former lavas erupted along the ridge during the spreading period of the SCS, whereas the latter magmas erupted in the seamounts after the cessation of the SCS opening (<14 Ma). On a plot of $^{207}Pb/^{204}Pb$ vs $^{206}Pb/^{204}Pb$, the SCS basalts broadly fall on the mixing array formed by DMM and 1·5 Ga recycled oceanic materials (Fig. 7b). In particular, the OIB-type basalts from the SCS possess radiogenic Pb isotopic compositions similar to those of the outer belt lavas in SE China (Figs 7b and 16). This indicates that the source of the SCS basalts also contained ancient ROC, and the contribution of ROC was diluted in the SCS MORB, probably owing to the higher extent of melting in shallower mantle relative to those seamount basalts.

Generally, plausible environments to isolate recycled materials for a long time may be the thermal boundary layer of the MTZ or CMB, which are likely to be slab 'graveyards' (e.g. Hirose *et al.*, 1999). The ROC was then incorporated into an upwelling flow and delivered to the melting region in the shallow asthenosphere. If this is the case, the Hainan plume is an essential carrier transferring the recycled materials beneath this island and adjacent regions (Fig. 17a and b; Zhang *et al.*, 2018). The low-velocity seismic anomaly beneath Hainan Island is rooted in the CMB (Zhao, 2007) and laterally dispersed across the upper mantle beneath the SCS (Fig. 17b). High-resolution seismic tomography revealed prominent high-velocity patches above the CMB, which support the presence of subducted oceanic crusts in the plume source region (He & Wen, 2011).

During the syn-spreading stage, intra-plate volcanism at the margin of SE China and Indochina was very rare with only sporadic volcanic pipes reaching the surface, as represented by the Jieyang basalts (*c.* 20 Ma) reported by Huang *et al.* (2013) and the Fuding basalts (*c.* 22 – 26 Ma) in this study (Fig. 17a). Given the similar geochemical and isotopic signatures of the concurrent volcanism at Jieyang and Fuding, we suggest that these lavas are related to a common source, consisting of ancient recycled oceanic materials and depleted mantle matrix. The oldest Cenozoic basalts in Hainan Island appeared at around 28·4 Ma (Sun, 1991). The above line of reasoning implies that the Hainan plume may have formed and dispersed beneath the lithosphere of SE China during the syn-spreading stage (Yu *et al.*, 2018; Zhang *et al.*, 2018). Here, we suggest that seafloor spreading during SCS opening would have caused a lateral mantle flow of the plume materials (Ito *et al.*, 2003) to primarily feed the ridge of the SCS during 32 – 16 Ma. This explains why intra-plate magmatism on the continental margins surrounding the SCS was sparse during this period.

Fundamental questions remaining are when and how the Hainan plume initiated? It has been proposed that the Izanagi–Pacific plate broke up in the MTZ and sank into the lower mantle at *c.* 50 Ma (Seton *et al.*, 2015; Kimura *et al.*, 2018). At this time, the motion of the Pacific plate changed from NNW to WNW, which was deduced from the alignment of the Hawaii–Emperor chain (Sharp & Clague, 2006). Meanwhile, the Indian and Eurasian plates collided, which facilitated the seaward rollback of the subducted Pacific slab (Yan *et al.*, 2008). The sinking of the Izanagi–Pacific slab could have induced convection in the overlying mantle, resulting in an upwelling of mantle with the dense crustal lithologies (Nakamura *et al.*, 1986). It could have also triggered a thermal instability in the lower mantle and thus the formation of a thermo-chemical plume (Li & Zhong, 2009). With this in mind, the area beneath Hainan Island can be considered unique in having a continuous low-velocity structure extending from the surface down to the CMB (Montelli *et al.*, 2006; Zhao, 2007). We suggest that the initiation of the Hainan plume may be a response to prolonged subduction of the (paleo-) Pacific plate. With the assumptions of its derivation from the CMB (2900 km depth) and the initiation at 50 Myr ago, the upwelling velocity of Hainan plume is calculated to be 15 cm a^{-1}, comparable with the upwelling velocity estimated for the Hawaii plume (10 – 30 cm a^{-1}; Sims *et al.*, 1999). Another study estimated a rather slow upwelling rate (<1 cm a^{-1}) for the Holocene alkaline basalts (<0·35 Ma) in Hainan Island, based on U-series disequilibria (Zou & Fan, 2010). The difference in the upwelling velocity between our estimation and the result of Zou & Fan (2010) may suggest that the strength of plume upwelling has declined with time during the last 50 Myr.

Post-spreading stage: Pacific subduction contributes to geochemical distribution

The basaltic volcanism reached a peak on the margin of SE China and the Indochina peninsula when opening of the SCS ceased. Given that Hainan Island is the geophysically detected thermal center, the similarity of isotopic compositions between basaltic lavas from Mingxi, Zhanjiang, Hainan Island, and the Indochina peninsula suggests that they were derived from a common source at the innermost core of the plume (Fig. 17a). The varying contributions of the subducted Pacific material in the melting regions could be responsible for the large isotopic variations in these lavas. In the regions close to the Pacific subduction zone, lavas from Zhangzhou as well as the seamounts in the SCS are characterized by higher $^{206}Pb/^{204}Pb$ and lower $^{143}Nd/^{144}Nd$ values (Fig. 10), implying a significant contribution of ancient ROC in their source regions. Then, the spatial variation in isotopic composition in the post-spreading lavas might reflect the lateral geochemical heterogeneities within the Hainan plume: the component responsible for the lavas close to the Pacific subduction zone must be located on the periphery of the plume, and the component generating the lavas away from the Pacific subduction zone (Indochina peninsula, Hainan Island and

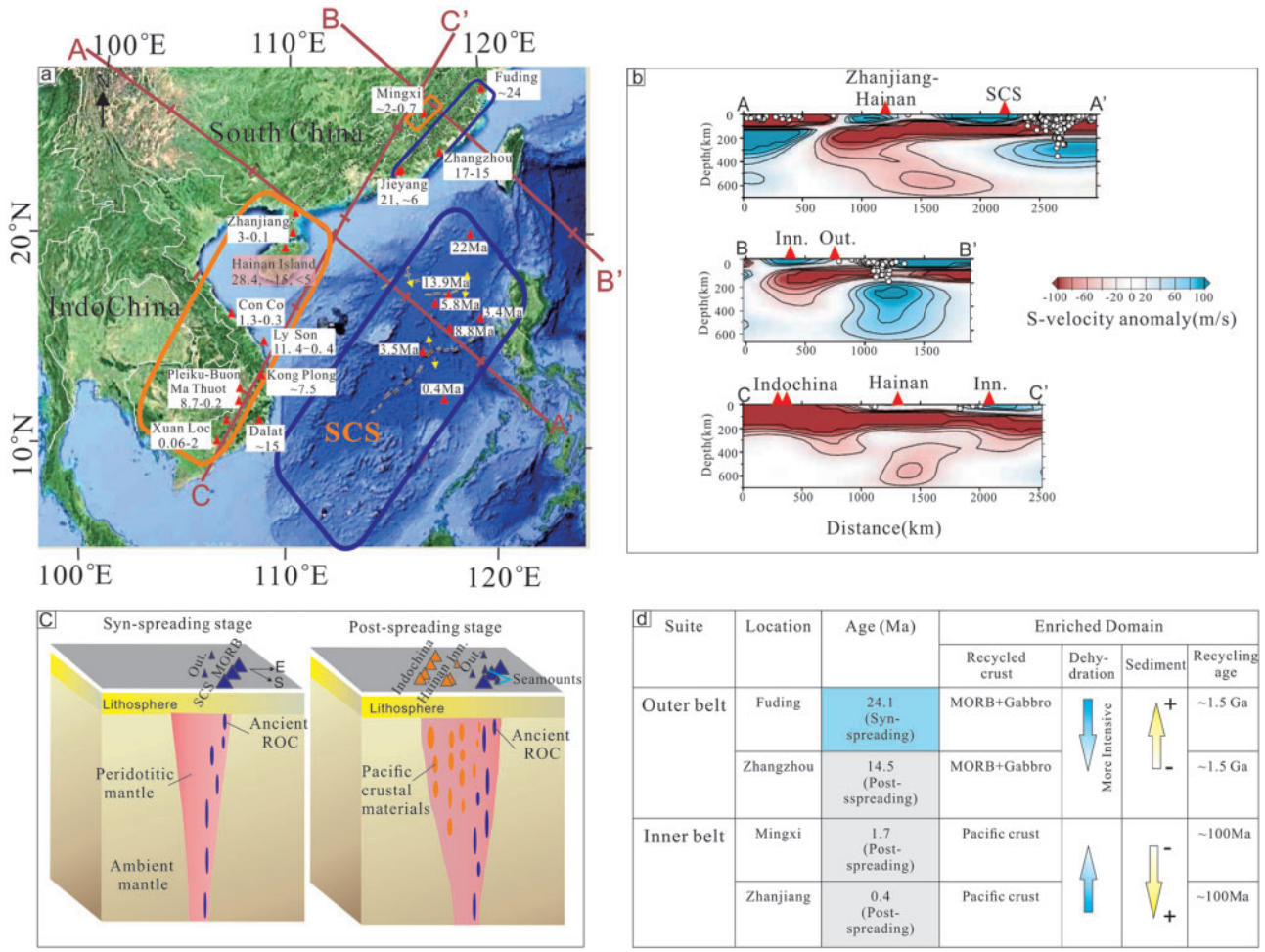

Suite	Location	Age (Ma)	Enriched Domain			
			Recycled crust	Dehydration	Sediment	Recycling age
Outer belt	Fuding	24.1 (Syn-spreading)	MORB+Gabbro	More Intensive	+	~1.5 Ga
	Zhangzhou	14.5 (Post-sspreading)	MORB+Gabbro		-	~1.5 Ga
Inner belt	Mingxi	1.7 (Post-spreading)	Pacific crust		-	~100Ma
	Zhanjiang	0.4 (Post-spreading)	Pacific crust		+	~100Ma

Fig. 17. (a) Map of SE China, the Indochina peninsula and the South China Sea (SCS) showing sample locations and volcano ages. The ranges of ages for each location, labeled with red triangles, are shown in a box near each of them. The age data for the basalts from Indochina are from An *et al.* (2017), Hoang *et al.* (2018) and the references therein, and the data for SE China basalts are same as shown in Fig. 3. The ages of seamount basalts of the SCS dated by Yan *et al.* (2006) are also shown. The volcanoes within purple and blue rectangles represent two geochemical groups, and the colors of the data symbols in the compositional and isotopic plots indicate the geochemical group from which a sample was taken. The three orange lines denote locations of the vertical cross-sections shown in (b). (b) Vertical cross-sections of the S-wave velocity anomaly along the three profiles shown in (a) (after Lebedev & Nolet, 2003). Contours are at ±40, ±60, ±80, and ±100 m s^{-1}. The abscissa values represent the distance from the starting point of each profile (e.g. A–A′) shown in (a). The interval between tick marks on the section lines is 500 km. The red triangles on the top denote locations of Cenozoic volcanoes from SE Asia. Inn., inner belt in SE China; Out., outer belt in SE China. (c) A conceptual model of the geochemical geometry of the Hainan plume. The compositions of the Hainan plume in different evolution stages and the associated volcanism in SE Asia are shown. The syn-spreading stage represents the period when the SCS seafloor was spreading (*c.* 32–16 Ma); the post-spreading stage represents the period from 16 Ma to the present. Colors of the volcanoes labelled by triangles atop the cylinder model correspond to the colors of their mantle components in the plume. This schematic model is modified after Jackson *et al.* (2014). (See main text for a detailed discussion.) (d) A brief summary of the enriched domains in the source of outer and inner belt lavas in SE China. The ages of the lavas shown here are the average values analyzed in this study.

the inner belt of SE China) must be located above the inner core of the plume. Lateral geochemical heterogeneity within mantle plumes has also been proposed for some hotspots; for example, Hawaii (Abouchami *et al.*, 2005; Tanaka *et al.*, 2008) and Samoa (Jackson *et al.*, 2014).

It is probably difficult to maintain geochemical zoning within a plume during its long-term upwelling (Ito *et al.*, 2003; Jackson *et al.*, 2014). However, numerical experiments have demonstrated that lateral heterogeneity within a plume caused by the spatial distribution of ROC materials in the peridotitic matrix can be preserved when the viscous plume materials ascend slowly (e.g. Albers & Christensen, 2001; Farnetani *et al.*, 2012). Such features are consistent with the characteristics postulated for the Hainan plume: (1) the very slow upwelling rate (Zou & Fan, 2010); (2) the low water content (84 – 360 ppm; Gu *et al.*, 2019), which resulted in high viscosity.

An episodic involvement of various-aged ROCs from different 'slab graveyards' further facilitated the preservation of the lateral geochemical heterogeneity within the Hainan plume. It is thought that the ancient oceanic crust was in the CMB (He & Wen, 2011) where the

plume is rooted (Wang *et al.*, 2013; Li *et al.*, 2014*b*), and the subducting Pacific slab is stagnant in the MTZ (Liu *et al.*, 2017). The first entrained ancient ROC remained on the periphery of the plume during upwelling, which fed the early formed basaltic lavas, similar to the model for the Samoan plume proposed by Jackson *et al.* (2014). The Pacific crustal materials were subsequently entrained when the plume transected the MTZ, embedded in the core of the Hainan plume, and contributed to the late-stage lavas (Fig. 17c). Dynamically, the asthenospheric upwelling is induced or assisted by deep subduction of the Pacific plate, above which large-scale mantle convection occurs (Huang & Zhao, 2006; Capitanio & Faccenda, 2012). Combined with the geophysical inference, we suggest that the upwelling beneath Hainan Island is initially dominated by CMB-rooted, hot flow, and then shows a gradation to a flow entraining MTZ materials. If this is the case, the existence of the Hainan plume could account for the regional-scale variations in isotopic compositions of the Cenozoic basalts from East China (Figs 1a and 7); the EM2-like isotopic characters in the SE China basalts are attributed to a CMB-rooted mantle upwelling, which contains both the ancient ROC and the Pacific crustal materials, whereas the EM1 signatures in the North and NE China basalts may have originated from an ancient, hydrated slab material in the MTZ (e.g. Kuritani *et al.*, 2011, 2019; Sakuyama *et al.*, 2013; Yang & Faccenda, 2020).

Surface expression of the plume-related magmatism

The classical examples of plume-related magmatism are always accompanied by large-volume eruptions of mafic magmas and formation of thick lava piles, as found in Hawaii, Iceland, or Ethiopia (White & McKenzie, 1995). By contrast, the volcanism in SE China produced dispersive eruptions of small-scale flows (Ho *et al.*, 2003; Zeng *et al.*, 2017; Figs 1, 2 and 17). Cenozoic volcanic fields are distributed along regional faults, which are subparallel to the coastline in SE China (23–26°N) (Fig. 2a). Ages of volcanic activity become younger inland (Fig. 3). It has been considered that the volcanism is associated with lithospheric extension induced by the persistent subduction of the Pacific plate that resulted in reactivation of pre-existing Mesozoic faults (Ma & Wu, 1987; Ren *et al.*, 2002; Huang & Xu, 2010). If this is the case, basaltic eruptions in SE China can be attributed to melting of mantle via decompression by localized lithospheric flexure or asthenospheric shear, rather than by a plume-driven upwelling (Hirano *et al.*, 2006; Brenna *et al.*, 2012*a*).

The extent of the thermal anomaly is a key factor in evaluating whether the volcanism is governed by a plume-driven upwelling (e.g. White & McKenzie, 1995; Campbell, 2007; Herzberg *et al.*, 2007). An excess mantle potential temperature of 100–200 K is estimated by petrological and seismic studies of the Hainan volcanic field (Wang *et al.*, 2012; Huang *et al.*, 2015; Wei & Chen, 2016), which supports the existence of an anomalously hot upwelling (i.e. plume). A larger-scale low-velocity anomaly connecting to this upwelling is observed below the lithosphere beneath SE China (Fig. 17b; Xia *et al.*, 2016), implying that much of the upper mantle has been infiltrated or replaced by warm upwelling materials. Integrating our geochemical and geochronological analyses and the geophysical observations, we suggest that the upwelling beneath Hainan Island impinged on the base of continental lithosphere and spread laterally along the lithosphere–asthenosphere boundary (Niu *et al.*, 2011; Gu *et al.*, 2019). Then, limited amounts of these stalling materials continue to rise along the weak zones (e.g. regional faults) in the lithosphere (Huang *et al.*, 2013), forming the small-scale, fault-related volcanoes in SE China.

Such a passive expression of plume materials driven by plate subduction is unusual globally, but it is due to the special tectonic setting, in which subducting slabs and a potential hotspot occur within about 1000 km of one another (Davaille *et al.*, 2005; Zhao *et al.*, 2011). The Hainan plume provides key insights into the interaction between plumes and plate subduction, and suggests that deep subduction of a plate can dynamically trigger mantle convection, resulting in local-scale plume upwelling (Lin & van Keken, 2006; Jackson *et al.*, 2017; Stracke *et al.*, 2019). The results reported here imply that the seismically detected Hainan plume represents a geochemically and lithologically anomalous column that is different from the ambient peridotitic mantle.

CONCLUSIONS

In this study, we collected late Cenozoic basaltic rocks from Fuding, Zhangzhou, Mingxi and Zhanjiang in SE China. The geochemical characteristics of these lavas provided a window through which we can understand the mantle evolution and geodynamic mechanisms operating beneath SE Asia since the late Paleogene. The major results of this work are as follows.

1. Together with previously published data, the K–Ar dating in this study indicates that after the cessation of the South China Sea opening (<16 Ma), the volcanism in SE China becomes younger from coastal to inland areas. Meanwhile, the SE China lavas show a spatial increase in $^{143}Nd/^{144}Nd$ ratios and decrease in $^{206}Pb/^{204}Pb$ and $^{87}Sr/^{86}Sr$ ratios with distance from the Pacific trench.
2. The SE China basalts show wide variations in compositions, ranging from a tholeiitic to alkalic and strongly alkalic affinity. The variation in major oxides for the tholeiites and weakly alkaline basalts reveals that fractionation of olivine and clinopyroxene probably occurred during magmatic evolution. Crystal fractionation has little effect on the compositions of ultra-alkaline basalts with high MgO (>10 wt%) from Fuding and Mingxi.

3. The low CaO contents, high Fe/Mn ratios and various TiO_2 contents of calculated primary magmas for the SE China basalts are hard to explain by partial melting of a single peridotite. Alternatively, we propose that a mafic component such as pyroxenite or eclogite, which represents recycled oceanic crustal materials, was mixed into the peridotitic mantle as a source lithology.
4. SE China basalts exhibit OIB-like trace element features. The combined trace element and Sr–Nd–Pb isotopic signatures of the SE China basalts indicate that the mantle source contains a package of recycled oceanic crust (MORB and gabbro) with variable amounts of surface marine sediments that were unevenly dehydrated during subduction. The recycled oceanic materials in the mantle source of lavas from the coast (Fuding and Zhangzhou) are more dehydrated, and have older recycling ages than those of the lavas from the interior (Mingxi and Zhanjiang).
5. The Nd–Pb isotope evolution model demonstrates that dehydrated oceanic crust with a recycling age of 1·5 Ga was the predominant enriched domain in the source of coastal lavas (Fuding and Zhangzhou), among which the source materials of Fuding lavas contained more ancient sediments. The subducting Pacific slab played a dominant role in the source of inland lavas (Mingxi and Zhanjiang), and a greater amount of subducting sediments was included in the source of Zhanjiang lavas.
6. The correlation between the temporal–spatial distribution of the volcanism on the surface and the variation of ancient and young recycled materials in the mantle source implies a dynamic linkage between the Pacific plate subduction and the generation of the Hainan plume. Mantle convections induced by the sinking of the Paleo-Pacific slab into the deep mantle and persistent subduction of the modern Pacific plate beneath the Eurasian plate may drive Hainan plume upwelling. The intermittently upwelling Hainan plume entrained recycled oceanic materials of different ages that fed the source of the late Cenozoic lavas in SE Asia, including SE China, the Indochina peninsula and the South China Sea, and gave rise to the geographically related compositional heterogeneities of these lavas.

ACKNOWLEDGEMENTS

Paul T. Robinson is specially thanked for useful discussion and for improving the paper. We would like to thank Marco Brenna and two anonymous reviewers, and the editor Georg Zellmer for very thorough reviews and many constructive comments that significantly improved the paper. We appreciate many very helpful discussions with Professor Ryoji Tanaka and Christian Potiszil. We thank Gen-An Shao, Si-Jing Liu and Di Yin for the assistance during the field investigations. Masahiro Yamanaka and Kayo Tanaka are thanked for their technical support.

FUNDING

This study was supported by the National Natural Science Foundation of China (grants 41702057 and 41630317), China Postdoctoral Science Foundation (2017M612530) and the MEXT (Ministry of Education, Culture, Sports, Science and Technology).

SUPPLEMENTARY DATA

Supplementary data are available at *Journal of Petrology* online.

REFERENCES

Abouchami, W., Hofmann, A. W., Galer, S. J. G., Frey, F. A., Eisele, J. & Feigenson, M. (2005). Lead isotopes reveal bilateral asymmetry and vertical continuity in the Hawaiian mantle plume. *Nature* **434**, 851.

Aigner-Torres, M., Blundy, J., Ulmer, P. & Pettke, T. (2007). Laser ablation ICPMS study of trace element partitioning between plagioclase and basaltic melts: an experimental approach. *Contributions to Mineralogy and Petrology* **153**, 647–667.

Albers, M. & Christensen, U. R. (2001). Channeling of plume flow beneath mid-ocean ridges. *Earth and Planetary Science Letters* **187**, 207–220.

An, A. R., Choi, S. H., Yu, Y. & Lee, D. C. (2017). Petrogenesis of Late Cenozoic basaltic rocks from southern Vietnam. *Lithos* **272**, 192–204.

An, M. J. & Shi, Y. L. (2006). Lithospheric thickness of the Chinese continent. *Physics of the Earth and Planetary Intereriors* **159**, 257–266.

Bizimis, M., Griselin, M., Lassiter, J. C., Salters, V. J. & Sen, G. (2007). Ancient recycled mantle lithosphere in the Hawaiian plume: osmium–hafnium isotopic evidence from peridotite mantle xenoliths. *Earth and Planetary Science Letters* **257**, 259–273.

Brenna, M., Cronin, S. J., Smith, I. E., Maas, R. & Sohn, Y. K. (2012a). How small-volume basaltic magmatic systems develop: a case study from the Jeju Island Volcanic Field, Korea. *Journal of Petrology* **53**, 985–1018.

Brenna, M., Cronin, S. J., Smith, I. E., Sohn, Y. K. & Maas, R. (2012b). Spatio-temporal evolution of a dispersed magmatic system and its implications for volcano growth, Jeju Island Volcanic Field, Korea. *Lithos* **148**, 337–352.

Briais, A., Patriat, P. & Tapponnier, P. (1993). Updated interpretation of magnetic anomalies and seafloor spreading stages in the South China Sea: implications for the Tertiary tectonics of Southeast Asia. *Journal of Geophysical Research: Solid Earth* **98**, 6299–6328. https://doi.org/10.1029/92JB02280.

Byerly, B. L. & Lassiter, J. C. (2014). Isotopically ultradepleted domains in the convecting upper mantle: Implications for MORB petrogenesis. *Geology* **42**, 203–206.

Campbell, I. H. (2007). Testing the plume theory. *Chemical Geology* **241**, 153–176. https://doi.org/10.1016/j.chemgeo.2007.01.024.

Capitanio, F. A. & Faccenda, M. (2012). Complex mantle flow around heterogeneous subducting oceanic plates. *Earth and Planetary Science Letters* **353**, 29–37.

Castillo, P. R. (2015). The recycling of marine carbonates and sources of HIMU and FOZO ocean island basalts. *Lithos* **216**, 254–263.

Castillo, P. R., Floyd, P. A. & France-Lanord, C. (1992). Isotope geochemistry of Leg 129 basalt: Implications for the origin of the widespread Cretaceous volcanic event in the Pacific. In Larson, R.L., Lancelot, Y., *et al.*, *Proceedings of the Ocean Drilling Program*, **129**. College Station, TX: Ocean Drilling Program, pp. 405–413.

Chauvel, C. & Hémond, C. (2000). Melting of a complete section of recycled oceanic crust: trace element and Pb isotopic evidence from Iceland. *Geochemistry, Geophysics, Geosystems* **1**. https://doi.org/10.1029/92JB02280

Chen, D. & Zhang, J. (1992). Nd, Sr, Pb isotopes and K–Ar ages of basaltic rocks in Linghai and Mingxi, Fujian Province. *Acta Petrologica Sinica* **8**, 324–331 (in Chinese with English abstract).

Chen, L., Hu, J., Yang, D., Song, H. & Wang, Z. (2017). Kinematic models for the opening of the South China Sea: an upwelling divergent flow origin. *Journal of Geodynamics* **107**, 20–33.

Chen, L. H., Zeng, G., Jiang, S. Y., Hofmann, A. W., Xu, X. S. & Pan, M. B. (2009). Source of Anfengshan basalts: subducted lower crust in the Sulu UHP belt, China. *Earth and Planetary Science Letters* **286**, 426–435.

Choi, S. H., Mukasa, S. B., Kwon, S. T. & Andronikov, A. V. (2006). Sr, Nd, Pb and Hf isotopic compositions of late Cenozoic alkali basalts in South Korea: Evidence for mixing between the two dominant asthenospheric mantle domains beneath East Asia. *Chemical Geology* **232**, 134–151.

Danyushevsky, L. V. (2001), The effect of small amounts of H_2O on crystallisation of mid-ocean ridge and backarc basin magmas, *Journal of Volcanology and Geothermal Research* **110**, 265–280, doi:10.1016/S0377–0273(01)00213–X.

Danyushevsky, L. V. & Plechov, P. (2011). Petrolog 3: integrated software for modeling crystallization processes. *Geochemistry, Geophysics, Geosystems* **12**(**7**) . http://dx.doi.org/10.1029/2011GC003516.

Dasgupta, R. & Hirschmann, M. M. (2006). Melting in the Earth's deep upper mantle caused by carbon dioxide. *Nature* **440**, 659–662.

Dasgupta, R., Hirschmann, M. M. & Stalker, K. (2006). Immiscible transition from carbonate-rich to silicate-rich melts in the 3 GPa melting interval of eclogite + CO_2 and genesis of silica-undersaturated ocean island lavas. *Journal of Petrology* **47**, 647–671

Dasgupta, R., Hirschmann, M. M. & Smith, N. D. (2007). Partial melting experiments of peridotite + CO_2 at 3 GPa and genesis of alkalic ocean island basalts. *Journal of Petrology* **48**, 2093–2124

Dasgupta, R., Jackson, M. G. & Lee, C.-T. A. (2010). Major element chemistry of ocean island basalts—Conditions of mantle melting and heterogeneity of mantle source. *Earth and Planetary Science Letters* **289**, 377–392.

Davaille, A., Stutzmann, E., Silveira, G., Besse, J. & Courtillot, V. (2005). Convective patterns under the Indo-Atlantic 'box'. *Earth and Planetary Science Letters* **239**, 233–252.

Denis, C. M. M., Alard, O. & Demouchy, S. (2015). Water content and hydrogen behaviour during metasomatism in the uppermost mantle beneath Ray Pic volcano (Massif Central, France). *Lithos* **236**, 256–274.

Eisele, J., Sharma, M., Galer, S. J., Blichert-Toft, J., Devey, C. W. & Hofmann, A. W. (2002). The role of sediment recycling in EM-1 inferred from Os, Pb, Hf, Nd, Sr isotope and trace element systematics of the Pitcairn hotspot. *Earth and Planetary Science Letters* **196**, 197–212.

Elliott, T., Plank, T., Zindler, A., White, W. & Bourdon, B. (1997). Element transport from slab to volcanic front at the Mariana arc. *Journal of Geophysical Research: Solid Earth* **102**, 14991–15019.

Farnetani, C. G., Hofmann, A. W. & Class, C. (2012). How double volcanic chains sample geochemical anomalies from the lowermost mantle. *Earth and Planetary Science Letters* **359–360**, 240–247.

Feigenson, M. D., Bolge, L. L., Carr, M. J. & Herzberg, C. T. (2003). REE inverse modeling of HSDP2 basalts: evidence for multiple sources in the Hawaiian plume. *Geochemistry, Geophysics, Geosystems* **4**(**2**). https://doi.org/10.1029/2001GC000271

Feyissa, D. H., Shinjo, R., Kitagawa, H., Meshesha, D. & Nakamura, E. (2017). Petrologic and geochemical characterization of rift-related magmatism at the northernmost Main Ethiopian Rift: Implications for plume–lithosphere interaction and the evolution of rift mantle sources. *Lithos* **282**, 240–261.

Gale, A., Dalton, C. A., Langmuir, C. H., Su, Y. & Schilling, J. G. (2013). The mean composition of ocean ridge basalts. *Geochemistry, Geophysics, Geosystems* **14**, 489−518.

Gao, R., Lassiter, J. C. & Ramirez, G. (2017). Origin of temporal compositional trends in monogenetic vent eruptions: Insights from the crystal cargo in the Papoose Canyon sequence, Big Pine Volcanic Field, CA. *Earth and Planetary Science Letters* **457**, 227–237.

Gao, S., Rudnick, R. L., Yuan, H. L., Liu, X. M., Liu, Y. S., Xu, W. L., Ling, W. L., Ayers, J., Wang, X. C. & Wang, Q. H. .(2004). Recycling lower continental crust in the North China craton. *Nature*, **432**, 892.

Gasperini, D., Blichert-Toft, J., Bosch, D., Del Moro, A., Macera, P., Télouk, P. & Albarede, F. (2000). Evidence from Sardinian basalt geochemistry for recycling of plume heads into the Earth's mantle. *Nature* **408**, 701.

Ge, T. M., Chen, W. J., Xu, X., Lee, D. M., Fan, L. M., Lee, Q., Wen, S. Y. & Wang, X. .(1989). The geomagnetic polarity time scale of Quaternary for Leiqiong area—K–Ar dating and palaeomagnetic evidence from volcanic rocks. *Acta Geophysica Sinica* **32**, 550–557 (in Chinese with English abstract).

Grove, T. L., Holbig, E. S., Barr, J. A., Till, C. B. & Krawczynski, M. J. (2013), Melts of garnet lherzolite: Experiments, models and comparison to melts of pyroxenite and carbonated lherzolite. *Contributions to Mineralogy and Petrology* **166**, 887–910.

Gu, X. Y., Wang, P. Y., Kuritani, T., Hanski, E., Xia, Q. K. & Wang, Q. Y. (2019). Low water content in the mantle source of the Hainan plume as a factor inhibiting the formation of a large igneous province. *Earth and Planetary Science Letters* **515**, 221–230.

Han, J. W., Xiong, X. L. & Zhu, Z. Y. (2009). Geochemistry of late-Cenozoic basalts from Leiqiong area: the origin of EM2 and the contribution from sub-continental lithosphere mantle. *Acta Petrologica Sinica* **25**, 3208–3220 (in Chinese with English abstract).

Hanyu, T., Kawabata, H., Tatsumi, Y., Kimura, J. I., Hyodo, H. & Sato, K., Miyazaki, T., Chang, Q., Hirahara, Y., Takahashi, T., Senda, R. & Nakai, S. .(2014). Isotope evolution in the HIMU reservoir beneath St. Helena: Implications for the mantle recycling of U and Th. *Geochimica et Cosmochimica Acta* **143**, 232−252.

Hart, S. R., Blusztajn, J., Dick, H. J., Meyer, P. S. & Muehlenbachs, K. (1999). The fingerprint of seawater circulation in a 500-meter section of ocean crust gabbros. *Geochimica et Cosmochimica Acta* **63**, 4059–4080.

Hauff, F. K., Hoernle, K. & Schmidt, A. (2003). Sr–Nd–Pb composition of Mesozoic Pacific oceanic crust (Site 1149 and 801, ODP Leg 185): Implications for alteration of oceanic crust and the input into the Izu–Bonin–Mariana subduction system. *Geochemistry, Geophysics, Geosystems* **4**, 8913. https://doi.org/10.1029/2002GC000421.

He, Y. & Wen, L. (2011). Seismic velocity structures and detailed features of the D'' discontinuity near the core–mantle boundary beneath eastern Eurasia. *Physics of the Earth and Planetary Interiors* **189**, 176–184.

Heinonen, J. S., Carlson, R. W., Riley, T. R., Luttinen, A. V. & Horan, M. F. (2014). Subduction-modified oceanic crust mixed with a depleted mantle reservoir in the sources of the Karoo continental flood basalt province. *Earth and Planetary Science Letters* **394**, 229–241.

Herzberg, C. (2006). Petrology and thermal structure of the Hawaiian plume from Mauna Kea volcano. *Nature* **444**, 605–609.

Herzberg, C. (2011). Identification of source lithology in the Hawaiian and Canary Islands: Implications for origins. *Journal of Petrology* **52**, 113–146.

Herzberg, C. & Asimow, P. D. (2008). Petrology of some oceanic island basalts: PRIMELT2. XLS software for primary magma calculation. *Geochemistry, Geophysics, Geosystems* **9** (9). http://dx.doi.org/10.1029/2008gc002057.

Herzberg, C. & O'Hara, M. J. (2002). Plume-associated ultramafic magmas of Phanerozoic age. *Journal of Petrology* **43**, 1857–1883.

Herzberg, C., Asimow, P. D., Arndt, N., Niu, Y., Lesher, C. M., Fitton, J. G., Cheadle, M. J. & Saunders, A. D. (2007), Temperatures in ambient mantle and plumes: Constraints from basalts, picrites, and komatiites. *Geochemistry, Geophysics, Geosystems* **8**, Q02006, doi: 10.1029/2006GC001390.

Hirano, N., Takahashi, E., Yamamoto, J., Abe, N., Ingle, S. P., Kaneoka, I., Hirata, T., Kimura, J. I., Ishii, T., Ogawa, Y., Machida S. & Suyehiro, K. (2006). Volcanism in response to plate flexure. *Science* **313**, 1426–1428.

Hirose, K. & Kushiro, I. (1993). Partial melting of dry peridotites at high pressures: Determination of compositions of melts segregated from peridotite using aggregates of diamond. *Earth and Planetary Science Letters* **114**, 477–489.

Hirose, K., Fei, Y., Ma, Y. & Mao, H. (1999). The fate of subducted basaltic crust in the Earth's lower mantle. *Nature* **397**, 53–56.

Ho, K. S., Chen, J. C. & Juang, W. S. (2000). Geochronology and geochemistry of late Cenozoic basalts from the Leiqiong area, Southern China. *Journal of Asian Earth Sciences* **18**, 307–324.

Ho, K. S., Chen, J. C., Lo, C. H. & Zhao, H. L. (2003). ^{40}Ar–^{39}Ar dating and geochemical characteristics of late Cenozoic basaltic rocks from the Zhejiang–Fujian region, SE China: eruption ages, magma evolution and petrogenesis. *Chemical Geology* **197**, 287–318.

Hoang, T. H. A., Choi, S. H., Yu, Y., Pham, T. H., Nguyen, K. H. & Ryu, J. S. (2018). Geochemical constraints on the spatial distribution of recycled oceanic crust in the mantle source of late Cenozoic basalts, Vietnam. *Lithos* **296**, 382–395.

Hofmann, A. W. (1988). Chemical differentiation of the Earth—the relationship between mantle, continental-crust, and oceanic-crust. *Earth and Planetary Science Letters* **90**, 297–314.

Hofmann, A. W. & Jochum, K. P. (1996) Source characteristics derived from very incompatible trace elements in Mauna Loa and Mauna Kea basalts, Hawaii Scientific Drilling Project. *Journal of Geophysical Research: Solid Earth* **101**, 11831–11839.

Hofmann, A. W. & White, W. M. (1982). Mantle plumes from ancient oceanic crust. *Earth and Planetary Science Letters* **57**, 421–436.

Homrighausen, S., Hoernle, K., Hauff, F., Geldmacher, J., Wartho, J. A., van den Bogaard, P. & Garbe-Schönberg, D. (2018). Global distribution of the HIMU end member: Formation through Archean plume-lid tectonics. *Earth-Science Reviews* **182**, 85–101.

Huang, J. L. & Zhao, D. P. (2006). High-resolution mantle tomography of China and surrounding regions. *Journal of Geophysical Research: Solid Earth* **111**, B09305.

Huang, S. & Frey, F. A. (2005). Recycled oceanic crust in the Hawaiian plume: evidence from temporal geochemical variations within the Koolau shield. *Contributions to Mineralogy and Petrology* **149**, 556–575.

Huang, S., Frey, F. A., Blichert-Toft, J., Fodor, R. V., Bauer, G. R. & Xu, G. (2005). Enriched components in the Hawaiian plume: evidence from Kahoolawe Volcano, Hawaii. *Geochemistry, Geophysics, Geosystems* **6**, Q11006, http://dx.doi.org/10.1029/2005GC001012.

Huang, X. & Xu, Y. (2010). Thermal state and structure of the lithosphere beneath eastern China: a synthesis on basalt-borne xenoliths. *Journal of Earth Science* **21**, 711–730.

Huang, X. L., Xu, Y. G. & Liu, D. Y. (2004). Geochronology, petrology and geochemistry of the granulite xenoliths from Nushan, east China: implication for a heterogeneous lower crust beneath the Sino-Korean Craton. *Geochimica et Cosmochimica Acta* **68**, 127–149.

Huang, X. L., Niu, Y., Xu, Y. G., Ma, J. L., Qiu, H. N. & Zhong, J. W. (2013). Geochronology and geochemistry of Cenozoic basalts from eastern Guangdong, SE China: constraints on the lithosphere evolution beneath the northern margin of the South China Sea. *Contributions to Mineralogy and Petrology* **165**, 437–455.

Huang, Z., Zhao, D. & Wang, L. (2015). P wave tomography and anisotropy beneath Southeast Asia: Insight into mantle dynamics. *Journal of Geophysical Research: Solid Earth* **120**, 5154–5174.

Ito, G., Lin, J. & Graham, D. (2003). Observational and theoretical studies of the dynamics of mantle plume–mid-ocean ridge interaction. *Reviews of Geophysics* **41, 1017**.

Jackson, M. G., Hart, S. R., Koppers, A. A., Staudigel, H., Konter, J., Blusztajn, J., Kurz, M. & Russell, J. A. .(2007). The return of subducted continental crust in Samoan lavas. *Nature* **448**, 684.

Jackson, M. G., Hart, S. R., Konter, J. G., Kurz, M. D., Blusztajn, J. & Farley, K. A. (2014). Helium and lead isotopes reveal the geochemical geometry of the Samoan plume. *Nature* **514**, 355.

Jackson, M. G., Konter, J. G. & Becker, T. W. (2017). Primordial helium entrained by the hottest mantle plumes. *Nature* **542**, 340.

Janney, P. E. & Castillo, P. R. (1997). Geochemistry of Mesozoic Pacific mid-ocean ridge basalt: Constraints on melt generation and the evolution of the Pacific upper mantle. *Journal of Geophysical Research: Solid Earth* **102**, 5207–5229. https://doi.org/10.1029/96JB03810

Juang, W. S. & Ho, K. S. (1996). Geochemical study of volcanics from backarc basin and continental rifting environments. *Geological Society of China Annual Meeting Abstracts*, 113–117 (in Chinese).

Keshav, S., Gudfinnsson, G. H., Sen, G. & Fei, Y. (2004). High-pressure melting experiments on garnet clinopyroxenite and the alkalic to tholeiitic transition in ocean-island basalts. *Earth and Planetary Science Letters* **223**, 365–379.

Kessel, R., Schmidt, M. W., Ulmer, P. & Pettke, T. (2005). Trace element signature of subduction-zone fluids, melts and supercritical liquids at 120–180 km depth. *Nature* **437**, 724–727.

Kimura, J. I., Sakuyama, T., Miyazaki, T., Vaglarov, B. S., Fukao, Y. & Stern, R. J. (2018). Plume–stagnant slab–lithosphere interactions: Origin of the late Cenozoic intra-plate basalts on the East Eurasia margin. *Lithos* **300**, 227–249.

Kinzler, R. J., Grove, T. L. & Recca, S. I. (1990). An experimental study on the effect of temperature and melt composition on the partitioning of nickel between olivine and silicate melt. *Geochimica et Cosmochimica Acta* **54**, 1255–1265.

Kogiso, T., Tatsumi, Y. & Nakano, S. (1997). Trace element transport during dehydration processes in the subducted oceanic crust: 1. Experiments and implications for the origin of ocean island basalts. *Earth and Planetary Science Letters* **148**, 193–205.

Kogiso, T., Hirose, K. & Takahashi, E. (1998). Melting experiments on homogeneous mixtures of peridotite and basalt: application to the genesis of ocean island basalts. *Earth and Planetary Science Letters* **162**, 45–61.

Kuritani, T. & Nakamura, E. (2003). Highly precise and accurate isotopic analysis of small amounts of Pb using ^{205}Pb–^{204}Pb and ^{207}Pb–^{204}Pb, two double spikes. *Journal of Analytical Atomic Spectrometry* **18**, 1464–1470.

Kuritani, T., Ohtani, E. & Kimura, J. I. (2011). Intensive hydration of the mantle transition zone beneath China caused by ancient slab stagnation. *Nature Geoscience* **4**, 713–716.

Kuritani, T., Xia, Q. K., Kimura, J. I., Liu, J., Shimizu, K., Ushikubo, T., Zhao, D. P., Nakagawa, M. & , & Yoshimura, S. (2019). Buoyant hydrous mantle plume from the mantle transition zone. *Science Reports* **9**, 1–7.

Lassiter, J. C., Hauri, E. H., Reiners, P. W. & Garcia, M. O. (2000). Generation of Hawaiian post-erosional lavas by melting of a mixed lherzolite/pyroxenite source. *Earth and Planetary Science Letters* **178**, 269–284.

Lebedev, S. & Nolet, G. (2003). Upper mantle beneath Southeast Asia from S velocity tomography. *Journal of Geophysical Research* **108** (B1), doi:10.1029/2000JB000073.

Lei, J., Zhao, D., Steinberger, B., Wu, B., Shen, F. & Li, Z. (2009). New seismic constraints on the upper mantle structure of the Hainan plume. *Physics of the Earth and Planetary Interiors* **173**, 33–50.

Le Maitre, R. W., Streckeisen, A., Zanettin, B., Le Bas, M. J., Bonin, B., & Bateman, P. (Eds.), 2005. *Igneous rocks: a classification and glossary of terms: recommendations of the International Union of Geological Sciences Subcommission on the Systematics of Igneous Rocks*. Cambridge: Cambridge University Press, 36 pp.

Le Roux, V., Dasgupta, R. & Lee, C. T. A. (2011), Mineralogical heterogeneities in the Earth's mantle: Constraints from Mn, Co, Ni and Zn partitioning during partial melting. *Earth and Planetary Science Letters* **307**, 395–408, doi: 10.1016/j.epsl.2011.05.014.

Li, C. & van der Hilst, R. D. (2010). Structure of the upper mantle and transition zone beneath Southeast Asia from traveltime tomography. *Journal of Geophysical Research* **115**, B07308, doi:10.1029/2009JB006882.

Li, C. F., Xu, X., Lin, J. , et al. (2014a). Ages and magnetic structures of the South China Sea constrained by deep tow magnetic surveys and IODP Expedition 349. *Geochemistry, Geophysics, Geosystems* **15**, 4958–4983. https://doi.org/10.1002/2014GC005567

Li, H. Y., Xu, Y. G., Ryan, J. G. & Whattam, S. A. (2017a). Evolution of the mantle beneath the eastern North China Craton during the Cenozoic: Linking geochemical and geophysical observations. *Journal of Geophysical Research: Solid Earth* **122**, 224–246.

Li, M., McNamara, A. K. & Garnero, E. J. (2014b). Chemical complexity of hotspots caused by cycling oceanic crust through mantle reservoirs. *Nature Geoscience* **7**, 366.

Li, S. G., Yang, W., Ke, S., Meng, X., Tian, H., Xu, L., .He, Y., Huang, J. H., Wang, X. C., Xia, Q., Sun, W., Yang, X., Ren, Z. Y., Wei, H., Liu, Y., Meng, F. & Yan, J. (2017b). Deep carbon cycles constrained by a large-scale mantle Mg isotope anomaly in eastern China. *National Science Review* **4**, 111–120.

Li, Y. Q., Ma, C. Q., Robinson, P. T., Zhou, Q. & Liu, M. L. (2015). Recycling of oceanic crust from a stagnant slab in the mantle transition zone: Evidence from Cenozoic continental basalts in Zhejiang Province, SE China. *Lithos* **230**, 146–165.

Li, Y. Q., Ma, C. Q. & Robinson, P. T. (2016). Petrology and geochemistry of Cenozoic intra-plate basalts in east–central China: Constraints on recycling of an oceanic slab in the source region. *Lithos* **262**, 27–43.

Li, Z.-X. & Zhong, S. (2009). Supercontinent–superplume coupling, true polar wander and plume mobility: plate dominance in whole-mantle tectonics. *Physica of the Earth and Planetary Interiors* **176**, 143–156.

Lin, S. C. & van Keken, P. E. (2006). Dynamics of thermochemical plumes: 2. Complexity of plume structures and its implications for mapping mantle plumes. *Geochemistry, Geophysics, Geosystems* **7**, Q03003.

Liu, J. Q., Ren, Z. Y., Nichols, A. R., Song, M. S., Qian, S. P., Zhang, Y. & Zhao, P. P. (2015). Petrogenesis of Late Cenozoic basalts from North Hainan Island: Constraints from melt inclusions and their host olivines. *Geochimica et Cosmochimica Acta* **152**, 89–121.

Liu, X., Zhao, D., Li, S. & Wei, W. (2017). Age of the subducting Pacific slab beneath East Asia and its geodynamic implications. *Earth and Planetary Science Letters* **464**, 166–174.

Liu, Y., Gao, S., Kelemen, P. B. & Xu, W. (2008). Recycled crust controls contrasting source compositions of Mesozoic and Cenozoic basalts in the North China Craton. *Geochimica et Cosmochimica Acta* **72**, 2349–2376.

Liu, Y. S., Gao, S., Yuan, H. L., Zhou, L., Liu, X. M., Wang, X. C., Hu, Z. & Wang L. .(2004). U–Pb zircon ages and Nd, Sr, Pb isotopes of lower crustal xenoliths from North China Craton: insights on evolution of lower continental crust. *Chemical Geology* **211**, 87–109.

Lu, Y., Makishima, A. & Nakamura, E. (2007). Coprecipitation of Ti, Mo, Sn and Sb with fluorides and application to determination of B, Ti, Zr, Nb, Mo, Sn, Sb, Hf and Ta by ICPMS. *Chemical Geology* **236**, 13–26.

Ma, X. & Wu, D. (1987). Cenozoic extensional tectonics in China. *Tectonophysics* **133**, 243–255.

Makishima, A. & Masuda, A. (1994). Ce isotope ratios of N-type MORB. *Chemical Geology* **118**, 1–8.

Makishima, A. & Nakamura, E. (2006). Determination of major/minor and trace elements in silicate samples by ICP-QMS and ICP-SFMS applying isotope dilution-internal standardization (ID-IS) and multi-stage internal standardisation. *Geostandards and Geoanalytical Research* **30**, 245–271.

Marín-Cerón, M. I., Moriguti, T., Makishima, A. & Nakamura, E. (2010). Slab decarbonation and CO_2 recycling in the southwestern Colombian volcanic arc. *Geochimica et Cosmochimica Acta* **74**, 1104–1121.

McDonald, G. A. & Katsura, T. (1964). Chemical composition of Hawaiian Lavas. *Journal of Petrology* **5**, 82–133.

McDonough, W. F. & Sun, S. S. (1995). The composition of the Earth. *Chemical Geology* **120**, 223–253.

Montelli, R., Nolet, G., Dahlen, F. A. & Masters, G. (2006). A catalogue of deep mantle plumes: New results from

finite-frequency tomography. *Geochemistry, Geophysics, Geosystems* **7**, Q11007.

Moon, V. & Jayawardane, J. (2004). Geomechanical and geochemical changes during early stages of weathering of Karamu Basalt, New Zealand. *Engineering Geology* **74**, 57–72.

Nagao, K., Ogata, A., Miura, Y. N. & Yamaguchi, K. (1996). Ar isotope analysis for K–Ar dating using two modified-VG5400 mass spectrometers—I: Isotope dilution method. *Journal of Mass Spectrometry Society of Japan* **44**, 39–61.

Nakamura, E., McDougall, I. & Campbell, I. H. (1986). K–Ar ages of basalts from the Higashi–Matsuura district, northwestern Kyushu, Japan and regional geochronology of the Cenozoic alkaline volcanic rocks in eastern Asia. *Geochemical Journal* **20**, 91–99.

Nakamura, E., Makishima, A., Moriguti, T., Kobayashi, K., Sakaguchi, C., Yokoyama, T., Tanaka, R., Kuritani, T. & Takei, H. .(2003). Comprehensive geochemical analysis of small amounts ($<$100 mg) of extraterrestrial samples for the analytical competition related to the sample return mission MUSES-C. *Institute of Space and Astronautical Science Report SP*, **16**, 49–101.

Nebel, O., Arculus, R., van Westrenen, W., Woodhead, J. D., Jenner, F. E., Nebel-Jacobsen, Y. J., Wille, M. & Eggins, S. M. .(2013). Coupled Hf–Nd–Pb isotope co-variations of HIMU oceanic island basalts from Mangaia, Cook–Austral islands, suggest an Archean source component in the mantle transition zone. *Geochimica et Cosmochimica Acta* **112**, 87–101.

Nier, A. O. (1950). A redetermination of the relative abundances of the isotopes of carbon, nitrogen, oxygen, argon, and potassium. *Physics Review* **77**, 789–793.

Niu, Y. (2018). Origin of the LLSVPs at the base of the mantle is a consequence of plate tectonics—A petrological and geochemical perspective. *Geoscience Frontiers* **9**, 1265–1278.

Niu, Y. & O'Hara, M. J. (2003). Origin of ocean island basalts: a new perspective from petrology, geochemistry, and mineral physics considerations. *Journal of Geophysical Research: Solid Earth* **108**, 2209.

Niu, Y., Wilson, M., Humphreys, E. R. & O'Hara, M. J. (2011). The origin of intra-plate ocean island basalts (OIB): the lid effect and its geodynamic implications. *Journal of Petrology* **52**, 1443–1468.

Niu, Y. L. (2014). Geological understanding of plate tectonics: basic concepts, illustrations, examples and new perspectives. *Global Tectonics and Metallogeny* **10**, 23–46.

Pertermann, M. & Hirschmann, M. M. (2003). Anhydrous partial melting experiments on MORB-like eclogite: phase relations, phase compositions and mineral–melt partitioning of major elements at 2–3 GPa. *Journal of Petrology* **44**, 2173–2201.

Pertermann, M., Hirschmann, M. M., Hametner, K., Günther, D. & Schmidt, M. W. (2004). Experimental determination of trace element partitioning between garnet and silica-rich liquid during anhydrous partial melting of MORB-like eclogite. *Geochemistry, Geophysics, Geosystems* **5**(**5**).

Pietruszka, A. J., Norman, M. D., Garcia, M. O., Marske, J. P. & Burns, D. H. (2013). Chemical heterogeneity in the Hawaiian mantle plume from the alteration and dehydration of recycled oceanic crust. *Earth and Planetary Science Letters* **361**, 298–309.

Pilet, S. (2015). Generation of low-silica alkaline lavas: Petrological constraints, models, and thermal implications. In: The interdisciplinary Earth: A volume in Honor of Don L. Anderson: *Geological Society of America Special Paper* **514**, 514–517.

Pilet, S., Baker, M. B. & Stolper, E. M. (2008). Metasomatized lithosphere and the origin of alkaline lavas. *Science* **320**, 916–919.

Pineda-Velasco, I., Kitagawa, H., Nguyen, T. T., Kobayashi, K. & Nakamura, E. (2018). Production of high-Sr andesite and dacite magmas by melting of subducting oceanic lithosphere at propagating slab tears. *Journal of Geophysical Research: Solid Earth* **123**, 3698–3728.

Plank, T. (2014). The chemical composition of subducting sediments. In: Holland, H. D. & Turekian, K. K. (Eds.), .*Treatise on Geochemistry*, **4**, 2nd edn. Oxford: Elsevier, pp. 607–629.

Plank, T. & Langmuir, C. H. (1998). The chemical composition of subducting sediment and its consequences for the crust and mantle. *Chemical Geology* **145**, 325–394.

Qi, Q., Taylor, L. A. & Zhou, X. (1995). Petrology and geochemistry of mantle peridotite xenoliths from SE China. *Journal of Petrology* **36**, 55–79.

Qin, L. & Humayun, M. (2008). The Fe/Mn ratio in MORB and OIB determined by ICP-MS. *Geochimica et Cosmochimica Acta* **72**, 1660–1677, doi:10.1016/j.gca.2008.01.012.

Ren, J., Tamaki, K., Li, S. & Junxia, Z. (2002). Late Mesozoic and Cenozoic rifting and its dynamic setting in Eastern China and adjacent areas. *Tectonophysics* **344**, 175–205.

Robinson, J. A. C. & Wood, B. J. (1998). The depth of the spinel to garnet transition at the peridotite solidus. *Earth and Planetary Science Letters* **164**, 277–284.

Roeder, P. & Emslie, R. F. (1970) Olivine–liquid equilibrium. *Contributions to Mineralogy and Petrology* **29**, 275–289.

Rudnick, R. L. & Gao, S. (2003). Composition of the continental crust. In: Rudnick, R. L., *The Crust. Treatise on Geochemistry*, **3**. Oxford: Elsevier, pp. 1–64.

Sakuyama, T., Tian, W., Kimura, J. I., Fukao, Y., Hirahara, Y., Takahashi, T., Senda, R., Chang, Q., Miyazaki, T., Obayashi, M., Kawabata, H. & Tatsumi, Y. .(2013). Melting of dehydrated oceanic crust from the stagnant slab and of the hydrated mantle transition zone: Constraints from Cenozoic alkaline basalts in eastern China. *Chemical Geology* **359**, 32–48.

Scott, J. M., Brenna, M., Crase, J. A., Waight, T. E., van der Meer, Q. H., Cooper, A. F., Palin, M. J., Le Roux, P. & Münker, C. (2016). Peridotitic lithosphere metasomatized by volatile-bearing melts, and its association with intraplate alkaline HIMU-like magmatism. *Journal of Petrology* **57**, 2053–2078.

Seton, M., Flament, N., Whittaker, J., Müller, R. D., Gurnis, M. & Bower, D. J. (2015). Ridge subduction sparked reorganization of the Pacific plate–mantle system 60–50 million years ago. *Geophysical Research Letters* **42**, 1732–1740.

Sharp, W. D. & Clague, D. A. (2006). 50-Ma initiation of Hawaiian–Emperor bend records major change in Pacific plate motion. *Science* **313**, 1281–1284.

Shi, X., Kohn, B., Spencer, S., Guo, X., Li, Y., Yang, X., Shi, H. & Gleadow, A. (2011). Cenozoic denudation history of southern Hainan Island, South China Sea: constraints from low temperature thermochronology. *Tectonophysics* **504**, 100–115.

Sims, K. W. W., DePaolo, D. J., Murrell, M. T., Baldredge, W. S., Goldstein, S., Clague, D. & Jull, M., (1999). Porosity of the melting zone and variations in the solid mantle upwelling rate beneath Hawaii: inferences from ^{238}U–^{230}Th–^{226}Ra and ^{235}U–^{231}Pa disequilibria. *Geochimica et Cosmochimica Acta* **63**, 4119–4138.

Skulski, T., Minarik, W. & Watson, E. B. (1994). High-pressure experimental trace-element partitioning between clinopyroxene and basaltic melts. *Chemical Geology* **117**, 127–147.

Slater, L., Jull, M., McKenzie, D. & Gronvöld, K. (1998). Deglaciation effects on mantle melting under Iceland: results from the northern volcanic zone. *Earth and Planetary Science Letters* **164**, 151–164.

Smith, I. E. M. & Németh, K. (2017). Source to surface model of monogenetic volcanism: a critical review. In: K. Németh, G. Carrasco-Nuñez, J. J. Aranda-Gómez, I. E. M. Smith (Eds.), Monogenetic Volcanism, *Geological Society, London, Special Publications*, **446**, 1–28.

Sobolev, A. V., Hofmann, A. W., Kuzmin, D. V. et al. . (2007). The amount of recycled crust in sources of mantle-derived melts. *Science* **316**, 412–417.

Sobolev, A. V., Hofmann, A. W., Jochum, K. P., Kuzmin, D. V. & Stoll, B. (2011). A young source for the Hawaiian plume. *Nature* **476**, 434–437.

Stacey, J. T. & Kramers, 1. (1975). Approximation of terrestrial lead isotope evolution by a two-stage model. *Earth and Planetary Science Letters* **26**, 207–221.

Staudigel, H., Plank, T., White, W. M. & Schmincke, H. U. (1996). Geochemical fluxes during seafloor alteration of the basaltic upper crust: DSDP sites 417 and 418. In: Bebout, G. E. & Kirby, S. H. (Eds), SUBCON: *Subduction from Top to Bottom. American Geophysical Union, Geophysical Monograph* **96**, 19–38.

Stracke, A. (2012). Earth's heterogeneous mantle: a product of convection-driven interaction between crust and mantle. *Chemical Geology* **330**, 274–299.

Stracke, A., Bizimis, M. & Salters, V. J. M. (2003). Recycling oceanic crust: quantitative constraints. *Geochemistry, Geophysics, Geosystems* **4** (3). https://doi.org/10.1029/2001GC000223.

Stracke, A., Hofmann, A. W. & Hart, S. R. (2005). FOZO, HIMU, and the rest of the mantle zoo. *Geochemistry, Geophysics, Geosystems* **6** (5). https://doi.org/10.1029/2004GC000824.

Stracke, A., Genske, F., Berndt, J. & Koornneef, J. M. (2019). Ubiquitous ultra-depleted domains in Earth's mantle. *Nature Geoscience* 12 (10), 1–5.

Su, B.-X., Hu, Y., Teng, F.-Z., Xiao, Y., Zhou, X.-H., Sun, Y., Zhou, M.-F. & Chang, S.-C. (2017). Magnesium isotope constraints on subduction contribution to Mesozoic and Cenozoic East Asian continental basalts. *Chemical Geology* **466**, 116–122.

Sun, J. S. (1991). Cenozoic volcanic activity in the northern south China Sea and Guangdong coastal area. *Marine Geology and Quaternary Geology* **11**, 45–67 (in Chinese with English abstract).

Sun, P., Niu, Y., Guo, P., Ye, L., Liu, J. & Feng, Y. (2017). Elemental and Sr–Nd–Pb isotope geochemistry of the Cenozoic basalts in Southeast China: Insights into their mantle sources and melting processes. *Lithos* **272**, 16–30.

Sun, S. S. & McDonough, W. F. (1989). Chemical and isotopic systematics of oceanic basalts: implications for mantle composition and processes. In: Saunders, A. D., & Norry, M. J. (eds) *Magmatism in the Ocean Basins. Geological Society, London, Special Publications* **42**, 313–345.

Tackley, P. J. (2011). Living dead slabs in 3-D: The dynamics of compositionally-stratified slabs entering a "slab graveyard" above the core–mantle boundary. *Physics of the Earth and Planetary Interiors* **188**, 150–162.

Takei, H. (2002). Development of precise analytical techniques for major and trace element concentrations in rock samples and their applications to the Hishikari gold mine, southern Kyushu, Japan. PhD thesis, Okayama University, Okayama.

Tanaka, R., Makishima, A., Kitagawa, H. & Nakamura, E. (2003). Suppression of Zr, Nb, Hf and Ta coprecipitation in fluoride compounds for determination in Ca-rich materials. *Journal of Analytical Atomic Spectrometry* **18**, 1458–1463.

Tanaka, R., Makishima, A. & Nakamura, E. (2008). Hawaiian double volcanic chain triggered by an episodic involvement of recycled material: constraints from temporal Sr–Nd–Hf–Pb isotopic trend of the Loa-type volcanoes. *Earth and Planetary Science Letters* **265**, 450–465.

Tatsumoto, M., Basu, A. R., Wankang, H., Junwen, W. & Guanghong, X. (1992). Sr, Nd, and Pb isotopes of ultramafic xenoliths in volcanic rocks of Eastern China: enriched components EMI and EMII in subcontinental lithosphere. *Earth and Planetary Science Letters* **113**, 107–128.

Tsay, A., Zajacz, Z., Ulmer, P. & Sanchez-Valle, C. (2017). Mobility of major and trace elements in the eclogite–fluid system and element fluxes upon slab dehydration. *Geochimica et Cosmochimica Acta* **198**, 70–91.

Tuff, J., Takahashi, E. & Gibson, S. A. (2005). Experimental constraints on the role of garnet pyroxenite in the genesis of high-Fe mantle plume derived melts. *Journal of Petrology* **46**, 2023–2058.

Vidal, V. & Bonneville, A. (2004). Variations of the Hawaiian hot spot activity revealed by variations in the magma production rate. *Journal of Geophysical Research: Solid Earth* **109, B03104,** https://doi.org/10.1029/2003JB002559

Walter, M. J. (1998) Melting of garnet peridotite and the origin of komatiite and depleted lithosphere. *Journal of Petrology* **39**, 29–60.

Wang, X. C., Li, Z. X., Li, X. H., Li, J., Liu, Y. Long, W. G., Zhou, J. B. & & Wang. F. . (2012). Temperature, pressure, and composition of the mantle source region of late Cenozoic basalts in Hainan Island, SE Asia: a consequence of a young thermal mantle plume close to subduction zones? *Journal of Petrology* **53**, 177–233.

Wang, X. C., Li, Z. X., Li, X. H., Li, J., Xu, Y. G. & Li, X. H. (2013). Identification of an ancient mantle reservoir and young recycled materials in the source region of a young mantle plume: implications for potential linkages between plume and plate tectonics. *Earth and Planetary Science Letters* **377**, 248–259.

Wang, X. J., Chen, L. H., Hofmann, A. W., Mao, F. G., Liu, J. Q. & Zhong, Y. (2017). Mantle transition zone-derived EM1 component beneath NE China: Geochemical evidence from Cenozoic potassic basalts. *Earth and Planetary Science Letters* **465**, 16–28.

Wang, X. J., Chen, L. H., Hofmann, A. W., Hanyu, T., Kawabata, H., Zhong, Y., Xie, L. W., Shi, J. H., Miyazaki, T., Hirahara, Y., Takahashi, T., Senda, R., Chang, Q., Vaglarov, B. S. & Kimura, J. I. .(2018). Recycled ancient ghost carbonate in the Pitcairn mantle plume. *Proceedings of the National Academy of Sciences of the USA* **115**, 8682–8687.

Wei, S. S. & Chen, Y. J. (2016). Seismic evidence of the Hainan mantle plume by receiver function analysis in southern China. *Geophysical Reserch Letters* **43**, 8978–8985. https://doi.org/10.1002/2016GL069513.

Weis, D., Garcia, M. O., Rhodes, J. M., Jellinek, M. & Scoates, J. S. (2011). Role of the deep mantle in generating the compositional asymmetry of the Hawaiian mantle plume. *Nature Geoscience* **4**, 831.

Weiss, Y., Class, C., Goldstein, S. L. & Hanyu, T. (2016). Key new pieces of the HIMU puzzle from olivines and diamond inclusions. *Nature* **537**, 666–670.

White, R. S. & McKenzie, D. (1995). Mantle plumes and flood basalts. *Journal of Geophysical Research: Solid Earth* **100**, 17543–17585.

White, W. M. (2010). Oceanic island basalts and mantle plumes: the geochemical perspective. *Annual Review of Earth and Planetary Sciences* **38**, 133–160.

Willbold, M. & Stracke, A. (2006). Trace element composition of mantle end-members: implications for recycling of oceanic and upper and lower continental crust. *Geochemistry, Geophysics, Geosystems* **7**, Q04004. https://doi.org/10.1029/2005GC001005.

Willbold, M. & Stracke, A. (2010). Formation of enriched mantle components by recycling of upper and lower continental crust. *Chemical Geology* **276**, 188–197.

Workman, R. K. & Hart, S. R. (2005). Major and trace element composition of the depleted MORB mantle (DMM). *Earth and Planetary Science Letters* **231**, 53–72.

Wu, H. H., Tsai, Y. B., Lee, T. Y., Lo, C. H., Hsieh, C. H. & Toan, D. (2004). 3-D shear wave velocity structure of the crust and upper mantle in South China Sea and its surrounding regions by surface wave dispersion analysis. *Marine Geophysical Research* **25**, 5–27.

Xia, S., Zhao, D., Sun, J. & Huang, H. (2016). Teleseismic imaging of the mantle beneath southernmost China: New insights into the Hainan plume. *Gondwana Research* **36**, 46–56.

Xu, S., Unsworth, M. J., Hu, X. & Mooney, W. D. (2019). Magnetotelluric evidence for asymmetric simple shear extension and lithospheric thinning in South China. *Journal of Geophysical Research: Solid Earth* **124**, 104–124.

Xu, X. S., O'Reilly, S. Y., Griffin, W. L. & Zhou, X. (2000). Genesis of young lithospheric mantle in southeastern China: an LAM-ICPMS trace element study. *Journal of Petrology* **41**, 111–148.

Xu, X. S., O'Reilly, S. Y., Griffin, W. L. & Zhou, X. (2003). Enrichment of upper mantle peridotite: petrological, trace element and isotopic evidence in xenoliths from SE China. *Chemical Geology* **198**, 163–188.

Xu, Y., Wei, J., Qiu, H., Zhang, H. & Huang, X. (2012). Opening and evolution of the South China Sea constrained by studies on volcanic rocks: preliminary results and a research design. *Chinese Science Bulletin* **57**, 3150–3164.

Xu, Y., Li, H., Hong, L., Ma, L., Ma, Q. & Sun, M. (2018). Generation of Cenozoic intraplate basalts in the big mantle wedge under eastern Asia. *Science China: Earth Sciences* **61**, 869–886.

Xu, Y. G., Ma, J., Frey, F. A., Feigenson, M. D. & Liu, J. F. (2005). Role of lithosphere–asthenosphere interaction in the genesis of Quaternary alkali and tholeiitic basalts from Datong, western North China Craton. *Chemical Geology* **224**, 247–271.

Yan, P., Deng, H., Liu, H., Zhang, Z. & Jiang, Y. (2006). The temporal and spatial distribution of volcanism in the South China Sea region. *Journal of Asian Earth Sciences* **27**, 647–659.

Yan, Q. S., Shi, X. F., Wang, K. S., Bu, W. R. & Xiao, L. (2008). Major element, trace element, Sr–Nd–Pb isotopic studies of Cenozoic alkali basalts from the South China Sea. *Science China (Series D)* **51**, 550–566.

Yan, Q., Shi, X,, Metcalfe, I., Liu, S., Xu, T., Kornkanitnan, N., Sirichaiseth, T., Yuang, L., Zhang, Y. & Zhang, H. . (2018). Hainan mantle plume produced late Cenozoic basaltic rocks in Thailand, Southeast Asia. *Science Reports* **8**, 2640.

Yang, F., Huang, X. L., Xu, Y. G. & He, P. L. (2019). Plume–ridge interaction in the South China Sea: Thermometric evidence from Hole U1431E of IODP Expedition 349. *Lithos* **324**, 466–478.

Yang, J. & Faccenda, M. (2020). Intraplate volcanism originating from upwelling hydrous mantle transition zone. *Nature* **579**, 88–91.

Ying, J. F., Zhang, H. F. & Tang, Y. J. (2010). Lower crustal xenoliths from Junan, Shandong province and their bearing on the nature of the lower crust beneath the North China Craton. *Lithos* **119**, 363–376.

Yokoyama, T., Makishima, A. & Nakamura, E. (1999). Evaluation of the coprecipitation of incompatible trace elements with fluoride during silicate rock dissolution by acid digestion. *Chemical Geology* **157**, 175–187.

Yu, M., Yan, Y., Huang, C.-Y., Zhang, X., Tian, Z., Chen, W.-H. & Santosh, M. (2018). Opening of the South China Sea and upwelling of the Hainan plume. *Geophysical Research Letters* **45**, 2600–2609.

Zeng, G., Chen, L. H., Hofmann, A. W., Jiang, S. Y. & Xu, X. S. (2011). Crust recycling in the source of two parallel volcanic chains in Shandong, North China. *Earth and Planetary Science Letters* **302**, 359–368.

Zeng, G., Chen, L. H., Yu, X., Liu, J. Q., Xu, X. S. & Erdmann, S. (2017). Magma–magma interaction in the mantle beneath eastern China. *Journal of Geophysical Research: Solid Earth* **122**, 2763–2779. https://doi.org/10.1002/2017JB014023.

Zhang, G, Luo, Q., Zhao, J., Jackson, M. G., Guo, L. & Zhong, L. (2018). Geochemical nature of sub-ridge mantle and opening dynamics of the South China Sea. *Earth and Planetary Science Letters* **489**, 145–155.

Zhao, D. (2007), Seismic images under 60 hotspots: Search for mantle plumes. *Gondwana Research* **12**, 335–355, doi: 10.1016/j.gr.2007.03.001.

Zhao, D., Yu, S. & Ohtani, E. (2011). East Asia: Seismotectonics, magmatism and mantle dynamics. *Journal of Asian Earth Sciences* **40**, 689–709.

Zhou, X. H., Zhu, B. Q., Liu, R. X. & Chen, W. J. (1988). Cenozoic basaltic rocks in eastern China. In: Macdougall, J. D. (Eds), *Continental Flood Basalts*. Dordrecht: Springer, pp. 311−330.

Zhou, Z. M., Ma, C. Q., Wang, L. X., Che, S. G., Xie, C. F., Li, Y. & Liu, W. (2018). A source-depleted Early Jurassic granitic pluton from South China: Implication to the Mesozoic juvenile accretion of the South China crust. *Lithos* **300**, 278–290

Zhu, B. & Wang, H. (1989). Nd–Sr–Pb isotopic and chemical evidence for the volcanism with MORB−OIB source characteristics in the Leiqiong Areas, China. *Geochimica* **03**, 193–201 (in Chinese with English abstract)

Zindler, A. & Hart, S. (1986). Chemical geodynamics. *Annual Review of Earth and Planetary Sciences* **14**, 493–571.

Zou, H. & Fan, Q. (2010). U–Th isotopes in Hainan basalts: implications for sub-asthenospheric origin of EM2 mantle endmember and the dynamics of melting beneath Hainan Island. *Lithos* **116**, 145–152.

Zou, H., Zindler, A., Xu, X. & Qi, Q. (2000). Major, trace element, and Nd, Sr and Pb isotope studies of Cenozoic basalts in SE China: mantle sources, regional variations, and tectonic significance. *Chemical Geology* **171**, 33–47.